İSTANBUL TECHNICAL UNIVERSITY ★ GRADUATE SCHOOL OF SCIENCE ENGINEERING AND TECHNOLOGY

INVESTIGATION OF BIOPARTICLE SEPARATION IN MICROFLUIDICS USING MICROPILLAR ARRAYS

M.Sc. THESIS

Reza DARYANI

Department of Mechanical Engineering

Heat and Fluid Program

JANUARY 2017

İSTANBUL TECHNICAL UNIVERSITY ★ GRADUATE SCHOOL OF SCIENCE ENGINEERING AND TECHNOLOGY

INVESTIGATION OF BIOPARTICLE SEPARATION IN MICROFLUIDICS USING MICROPILLAR ARRAYS

M.Sc. THESIS

Reza DARYANI
(503131128)

Department of Mechanical Engineering

Heat and Fluid Program

Thesis Advisor: Prof. Dr. Lütfullah KUDDUSI

JANUARY 2017

İSTANBUL TEKNİK ÜNİVERSİTESİ ★ FEN BİLİMLERİ ENSTİTÜSÜ

DİREK DİZİLER KULLANILARAK MİKRO AKIŞKANLARDAKİ BİYOPARÇACIK AYRIŞTRILMASININ ARAŞTIRILMASI

YÜKSEK LİSANS TEZİ

Reza DARYANI
(503131128)

Makina Mühendisliği

Isı Akışkan Programı

Tez Danışmanı: Prof. Dr. Lütfullah KUDDUSI

OCAK 2017

Reza DARYANI, a M.Sc. student of İTU Graduate School of Science Engineering and Technology student ID 503131128, successfully defended the thesis entitled "INVESTIGATION OF BIOPARTICLE SEPARATION IN MICROFLUIDICS USING MICROPILLAR ARRAYS", which he prepared after fulfilling the requirements specified in the associated legislations, before the jury whose signatures are below.

Thesis Advisor :	**Prof. Dr. Lütfullah KUDDUSI** İstanbul Technical University	.....
Jury Members :	**Asst.Prof. Dr. Murat ÇAKAN** İstanbul Technical University	.....
	Assoc.Prof. Dr. Hakan DEMIR Yıldız Technical University	.....

Date of Submission : 28 November 2016
Date of Defense : 23 January 2017

To my dear family,

FOREWORD

I would like to express my deep appreciation and thanks for my advisor, Prof. Dr. Lütfullah KUDDUSI. This was impossible without his warm guidance, support and encouragement during the entire master study.

At the end, I would like to thanks my family for their warm support and love in my life.

November 2016

Reza DARYANI

(Mechanical engineer)

TABLE OF CONTENTS

Page

FOREWORD ..... **ix**
TABLE OF CONTENTS ..... **xi**
ABBREVIATIONS ..... **xiii**
SYMBOLS ..... **xv**
LIST OF TABLES ..... **xvii**
LIST OF FIGURES ..... **xix**
1. INTRODUCTION **1**
1.1 Literature Review 3
1.1.1 Background of studies in porous media 3
1.1.2 Background of microfluidic devices used for particle separation 5
1.2 Research Objectives 12
2. GOVERNING EQUATIONS AND THEORETICAL INVESTIGATIONS **13**
2.1 Navier-Stokes Equations 13
2.2 Darcy's Law 13
2.3 Brinkman's Equation 14
2.4 Theoretical Issues of Particle Interception 15
3. MODEL DESCRIPTION FOR PARAMETRIC STUDIES **21**
3.1 Model Definition for the Single Circular Solid Post 21
3.2 Model Definition for the Single Circular Porous Post 22
3.3 Models Definition for Various Shape of the Post 24
3.4 Model Definition for Configuration of the Posts 27
3.5 Model Definition for the Geometrical Parameters between the Posts 30
3.6 Blood Viscosity Models 31
4. RESULTS AND DISCUSSION **33**
4.1 Validation of the Numerical Solutions 33
4.2 Comparison of the Interception efficiency of Solid and Porous Posts 35
4.2.1 Interception efficiency of a Solid Post 35
4.2.2 Interception efficiency of a Porous Post 38
4.2.3 Investigation of the Streamlines Pattern 41
4.3 Investigation of the Effect of the Darcy Number: 42
4.3.1 Effect of Darcy number on different post diameter 42
4.3.2 Effect of the Darcy number on interception efficiency 43
4.4 Effect of the Different Materials of the Porous Post 44
4.5 Influence of the Shape of the Porous Post 45
4.6 Impact of the Configuration of the Porous Posts 48
4.7 Effect of the Geometrical Parameters between Posts 52
5. CONCLUSION **55**
6. REFERENCES **57**
CURRICULUM VITAE **61**

ABBREVIATIONS

MEMS	: Microelectromechanical Systems
NEMS	: Nanoelectromechanical Systems
PDMS	: Polydimethylsiloxane
CNT	: Carbon Nano Tubes
VCANT	: Vertically Aligned Carbon Nanotubes
FEM	: Finite-Element Method
CTC	: Circulating Tumor Cells
HIV	: Human Immunodeficiency Virus
SEM	: Scanning Electron Micrograph
MACS	: Magnetic Activated Cell Sorting
FACS	: Fluorescent Activated Cell Sorting

SYMBOLS

$\mathbf{v}$	: Velocity
$\boldsymbol{P}$	: Pressure
$\boldsymbol{\rho}$	: Density
$\boldsymbol{\mu}$	: Dynamic viscosity
$\boldsymbol{\kappa}$	: Permeability
$\mathbf{v}'$	: Non-dimensional velocity
$\boldsymbol{U}$	: Average velocity
$\boldsymbol{P}'$	: Non-dimensional mean pressure
$\boldsymbol{a}$	: Characteristic length
$\boldsymbol{Da}$	: Darcy number
$\widetilde{\boldsymbol{\mu}}$	: Effective viscosity
$\boldsymbol{\varphi}$	: Porosity
$\boldsymbol{\eta_i}$	: Direct interception efficiency
$\boldsymbol{b}$	: Upstream streamlines span
$\boldsymbol{d_c}$	: Post characteristic length
$\boldsymbol{\eta_{diff}}$	: Interception efficiency by Brownian diffusion
Pe	: Peclet number
L	: Channel length
D	: Diffusion coefficient
$\boldsymbol{k}$	: Boltzmann constant
T	: Temperature
$\boldsymbol{a_p}$	: Particle radius
$\boldsymbol{A_F}$	: Coefficient
$\boldsymbol{d_c}$	: Post width
$\boldsymbol{\nu}$	: Kinematic viscosity
$\boldsymbol{Stk}$	: Stoke's number
s	: Specific gravity
$\boldsymbol{d_p}$	: Particle diameter
H	: Hamaker constant
$\boldsymbol{N_{Ad}}$	: Adhesion coefficient
w	: Channel Width
c	: Airfoil chord
a	: Post characteristic length
l	: Distance between adjacent posts
$\boldsymbol{\alpha}$	: Distance between centers of posts
$\boldsymbol{\mu_0}$,$\boldsymbol{n}$, $\boldsymbol{\lambda}$	: Constants
$\dot{\boldsymbol{\gamma}}$	: Shear rate
$\boldsymbol{\mu_\infty}$	: Viscosity at high shear rate
$\boldsymbol{Re}$	: Reynolds number
$\boldsymbol{\eta}$	: Interception efficiency

LIST OF TABLES

Page

Table 3.1 : Geometrical parameters of Figure 3.1..... **21**
Table 3.2 : Geometrical parameters of Figure 3.3..... **23**
Table 3.3 : Values of geometrical parameters of Figure 3.5. ..... **25**
Table 3.4 : Values of geometrical parameters of Figure 3.6. ..... **26**
Table 3.5 : Values of geometrical parameters of Figure 3.7. ..... **26**
Table 3.6 : Values of geometrical parameters of Figure 3.8. ..... **27**
Table 3.7 : Properties of the model of Figure 3.11. ..... **28**
Table 3.8 : Properties of the model of Figure 3.12. ..... **29**
Table 3.9 : Properties of the model of Figure 3.13. ..... **30**
Table 3.10 : Properties of the model of Figure 3.14. ..... **30**
Table 3.11 : Geometrical parameters of Figure 3.15..... **31**
Table 3.12: Properties of working fluids..... **31**
Table 4.1 : Properties of the cases investigated by Chen et al. [2]..... **33**
Table 4.2 : Interception efficiency values of current work and by Chen et al. **34**
Table 4.3 : Geometrical properties of solid and porous posts models. **35**
Table 4.4 : Values of direct interception efficiency for the solid post. **36**
Table 4.5 : Values of interception efficiency for a solid post. **38**
Table 4.6 : Values of the direct interception efficiency for the porous post. **39**
Table 4.7 : Values of the interception efficiency for the porous post. **40**
Table 4.8 : Properties of the cases. **43**
Table 4.9 : Properties of the cases. **43**
Table 4.10 : Properties of the various materials used for the porous post [13]..... **45**

LIST OF FIGURES

Page

Figure 1.1 : Comparison of the capturing of bioparticles with nanoporous and solid collectors a) a single post b) post arrays. Inset boxes illustrate isolation on non-functionalized control devices [1]. **2**
Figure 1.2 : Comparison of a nanoporous and a solid post [1]. **3**
Figure 1.3 : Size and typical concentration of bioparticles present in the blood [13]. **6**
Figure 1.4 : Schematic of a channel of asymmetrically curved inertial focusing [15]. **7**
Figure 1.5 : Schematic illustration of particle separation by deterministic hydrodynamics [17]. **8**
Figure 1.6 : A microfluidic DEP cytometer; SEM (scanning electron micrograph) of a completed 1×8 trap array [19]..... **8**
Figure 1.7 : Schematic of a multilayer resonant structure [22]..... **9**
Figure 1.8 : a) Active magnetic separation device. b) Passive magnetic separation device [23]. **10**
Figure 1.9 : a) Schematic of the optical cell sorter instrument. b) The layout of the device [24]. **10**
Figure 1.10 : a) Schematic depiction of a CD4 counting device. b) Picture of a linear cell-counting device. c) Geometry of the device [27]. **11**
Figure 1.11 : Schematics of a device used for capturing CTCs [28]. **11**
Figure 2.1 : Schematic illustration of direct interception mechanism. **16**
Figure 2.2 : Schematic of a post for the definition of interception efficiency. **17**
Figure 2.3 : Schematic illustration of Brownian diffusion mechanism. **18**
Figure 2.4 : Schematic illustration of inertial impaction mechanism. **18**
Figure 2.5 : Schematic illustration of gravitational sedimentation. **19**
Figure 2.6 : Adjustment factor for interception efficiency based on N_{Ad}.(adapted from [35])..... Error! Bookmark not defined.
Figure 3.1 : Schematic model of the single solid post with a circular cross section inside a rectangular channel..... **21**
Figure 3.2 : Schematic of a single porous post with a circular cross section inside a rectangular channel. **22**
Figure 3.3 : Schematic model of the single circular porous post. **23**
Figure 3.4 : Schematic illustration of different posts cross sections..... **24**
Figure 3.5 : Schematic model of the single porous airfoil post. **25**
Figure 3.6 : Schematic model of the single porous truncated hexagon post..... **26**
Figure 3.7 : Schematic model of the single porous square post..... **26**
Figure 3.8 : Schematic model of the single porous regular hexagon post. **27**
Figure 3.9 : a) A schematic depiction of a cell-binding device. b) an exploded view of a cell-binding device of Figure a [37]. **27**

Figure 3.10 : a) A schematic illustration of a square array of circular posts. b) a schematic illustration of an equilateral triangle array of circular posts [37]. **27**
Figure 3.11 : Schematic models of the circular posts arrays in square and equilateral triangle forms. **28**
Figure 3.12 : Schematic models of the square posts arrays in square and equilateral triangle forms. **29**
Figure 3.13 : Schematic models of the truncated hexagonal posts arrays in square and equilateral triangle forms. **29**
Figure 3.14 : Schematic models of the regular hexagonal posts arrays in square and equilateral triangle forms. **30**
Figure 3.15 : Schematic illustration of the posts of the model. **31**
Figure 4.1 : Comparison between the interception efficiencies obtained from numerical simulations and measured by Chen et al. [2]. **35**
Figure 4.2 : Schematic illustration of the streamlines around the solid post with the distance less than 25 (μm) inside the channel. **37**
Figure 4.3 : Schematic illustration of the streamlines around the porous post with the distance less than 25 (μm) inside the channel. **40**
Figure 4.4 : Comparison of the interception efficiency of the solid and porous post. **41**
Figure 4.5 : Streamlines comparison for a) a solid post and b) a porous post. **41**
Figure 4.6 : Schematic illustration of posts of models a) $5\mu m$, b) $50\ \mu m$, and c) $500\ \mu m$. **42**
Figure 4.7 : Illustration of the constant Darcy number effect on streamlines pattern for different post sizes. (For better comparison, the smaller posts are scaled to the same size as the largest one.). **43**
Figure 4.8 : Impact of the different Darcy number on interception efficiency. **44**
Figure 4.9 : Interception efficiency of various porous materials for $dp/dc = 0.05, 0.1$. **45**
Figure 4.10 : Interception efficiency of the post with different shapes for water as working fluid. **46**
Figure 4.11 : Interception efficiency of the post with different shapes for the blood as working fluid. **47**
Figure 4.12 : Schematic of the flow streamlines of an airfoil post for a) water b) blood. **47**
Figure 4.13 : Schematic of the flow streamlines of a circular post for a) water b) blood. **48**
Figure 4.14 : Schematic of the flow streamlines of a truncated hexagon post for a) water b) blood. **48**
Figure 4.15 : Schematic of the flow streamlines of a square post for a) water b) blood. **48**
Figure 4.16 : Schematic of the flow streamlines of a regular hexagon post for a) water b) blood. **48**
Figure 4.17 : Interception efficiency of the post arrays in the square configuration for water. **49**
Figure 4.18 : Interception efficiency of the post arrays in the equilateral triangle configuration for water. **49**
Figure 4.19 : Interception efficiency of the post arrays in the square configuration for blood. **50**

Figure 4.20 : Interception efficiency of the post arrays in the equilateral triangle configuration for blood. **50**
Figure 4.21 : Plots of streamlines for post arrays with the regular hexagonal cross section for water. a) Square configuration b) Equilateral triangle configuration. The boxes indicate a higher concentration of streamlines for the square configuration. **51**
Figure 4.22 : Plots of streamlines for post arrays with the regular hexagonal cross section for blood. a) Square configuration b) Equilateral triangle configuration. **52**
Figure 4.23 : Variation of interception efficiency versus array density..... **53**

INVESTIGATION OF BIOPARTICLE SEPARATION IN MICROFLUIDICS USING MICROPILLAR ARRAYS

SUMMARY

Investigation of the factors causing disease is the primary aim of basic researches in the field of bioparticle separation and clinical diagnostics. In this respect, isolation of cells or biomolecules from more complex samples such as blood, sputum, saliva, etc. is required. Unfortunately, there are some limitations for these studies when the target bioparticles in the samples exist in very small quantities. Also, most of the current methods for bioparticle separation that are used in research and clinical laboratories, have been available for several decades. The majority of these methods need a large amount of sample, several manual steps, and could take hours to be done. They can be categorized into two groups: methods that are mainly based on differences in physical properties between particles, and methods that include specific biomolecular recognition.

Application of microfluidics as an essential tool in analysis and research in biological fields is increasing due to the advantages that it offers in bioparticle separation. The advantages such as lower cost, smaller sample amount, shorter separation duration, understandable fluid dynamics, and disposable devices. Currently, there are various types of microfluidic systems; however, they can be classified into two main groups: 1) Physical properties based platforms in microfluidic separation and 2) Specific biomolecular recognition based platforms in microfluidic separation.

One of the microfluidic devices that is used for isolation of bioparticles, consists of a rectangular microchannel in which micro-pillars' (or micro posts) array are located in the vertical direction with the height equal to the channel height. The used materials for fabrication of this bioseparation device can be either solid or porous materials.

For many applications in the field of bioparticle separation, efficient isolation of bioparticles is crucial. Isolation efficiency depends on two factors including the interception efficiency, and the binding efficiency. To clarify, the interception

efficiency is the fraction of particles in a flow that are intercepted by a collector, and the binding efficiency is the possibility of binding of the intercepted particles to the surface of a collector. Because of the fact that there is no evidence to suggest the measurement of the binding efficiency value, this thesis focuses on interception efficiency.

Interception of particles is studied in various realms of science such as biological particle capturing, air filtration, marine ecology, etc. The four principal mechanisms that are known as classical mechanisms contribute in particle interception including the direct interception, diffusion, inertial impaction, and gravitational sedimentation. In addition to the four mechanisms of particle interception, there are other important physical effects imposed by the post surface on a particle when it approaches the solid surface. The direct interception is a result of streamline kinematics. To explain, when a moving particle in a flow locates on a streamline that finally approaches the post with a distance less than the radius of the particle, it collides to the post and the direct interception occurs. Meanwhile, the most important factor in interception efficiency is the direct interception, and other factors have a negligible effect on interception efficiency.

Solid materials such as polymers, glass or silicon are used for constructing most of the microfluidic devices that are designed for particle separation. However, there are some restrictions for this type of devices. For example, low efficiency of particle capturing, limited function in isolation of sub-micron particles, and limitations in the application for various particle types. While, for suspended particles in a liquid, the isolation efficiency of a solid post is very low. The two reasons causing this are: 1) a bulk flow effect 2) a near-surface effect.

Utilization of porous materials could resolve the stated restrictions. A porous medium can be defined as a material consisting of a solid matrix with an interconnected void. There are two factors involved in the improvement of interception efficiency of a porous post in comparison with a solid one. The first factor is related to the changes in the flow field due to the use of the porous structure. In other words, by penetrating many more streamlines to the porous structure, a higher interception occurs. The other factor is the reduced hydrodynamic resistance of a porous post, which is assumed to have a negligible value for it.

The comparison between interception efficiency of a solid and porous post is investigated by developing a model of a single circular post inside a rectangular channel. Analysis showed that higher interception efficiency is achieved by using a porous material for the post. For further investigations, models are developed based on the parameters that would improve interception efficiency. Parameters such as the materials of porous structure, shape of the post, different configuration for post arrays, and geometrical parameters between post arrays.

Models are simulated by COMSOL Multiphysics (v5.2) software, which utilizes the finite element method (FEM). The governing equations for free media region are the continuity equation for the conservation of mass, and the 2-D Navier-Stokes equations for the conservation of momentum. Meanwhile, for flow regimes that completely are inside a porous structure, Darcy's law can be applied. However, for flow regimes that are a combination of free and porous media, Darcy's law is not so accurate. For analyzing such problems, modification of Darcy's law which was proposed by Brinkman commonly is used. Stated equations are solved for various models and different particles for two fluid types, which are water and blood. The flow is low Reynolds number laminar flow, and the solutions obtained for the steady state condition.

Results indicated that interception efficiency is significantly improved by selecting porous material for the post. Additionally, by choosing a hexagonal cross section, and a square configuration of the posts higher interception efficiency is achieved. Furthermore, the results revealed that using blood as the working fluid results in greater interception efficiency in comparison with water.

DIREK DIZILER KULLANILARAK MIKRO AKIŞKANLARDAKI BIYOPARÇACIK AYRIŞTIRILMASININ ARAŞTIRILMASI

ÖZET

Klinik tanı çalışmalarının ve biyomoleküllerin ayrıştırılmasının esas amacı hastalığın altında yatan nedenleri ortaya çıkartmaktır. Bunu yapabilmek için hastalığa özgü biyomolekül veya hücrelerden kan, tükürük, hücre kültürü gibi örnekler almak ve çeşitli tanecikleri izole etmek gerekmektedir. Ancak bu örneklerin miktarlarının az olduğu durumlarda araştırma yapma kabiliyetimiz sınırlanmaktadır. Ayrıca, araştırma ve klinik laboratuvarlarında biyotaneciklerin ayrıştırılmasında bir çok yöntem yıllardır kullanılmaktadır. Bu yöntemlerin bir çoğu büyük miktarda örnek gerektirmekte, bir çok adımda gerçekleşmekte ve sonuç alınması uzun zaman almaktadır. Bu yöntemleri iki gruba ayırmak mümkündür. Bunların ilki taneciklerin fiziksel özelliklerindeki farklara dayanmaktadır. İkinci gruptaki yöntemler ise biyotaneciklerin teşhisinden yararlanmaktadır.

Biyotaneciklerin ayrıştırılmasının avantajları mikro akışkan alanındaki gelişmelerden kaynaklanmaktadır. Avantajları arasında düşük maliyet, küçük örnek hacimlerinin yeterli olması, ayrıştırma zamanının kısa olması, akışkan hareketlerinin öngörülebilir olması ve tek kullanımlık aletler kullanılabilir olması sayılabilir. Sonuç olarak, çeşitli biyotanecikler için, çok çeşitli cihazlar kullanılmaktadır. Mikro akışkanların ayrıştırılmasında kullanılan yöntemler fiziksel özellik farkından ve tanecik belirlenmesinden yararlanmaktadır.

Biyomoleküllerin izolasyonun kullanılan mikro akışkan cihazlarından birinde akışa dik olan ve kanalın yüksekliği boyunca uzanan mikro direk dizilerine sahip dikdörtgen şeklinde mikro kanallar kullanılmaktadır. Biyomoleküllerin ayrıştırılmasında kullanılan bu gibi cihazlar genellikle cam, silikon, metal, polimer ve gözenekli malzemelerden yapılmaktadır.

Biyomedikal araştırmalarda ve klinik teşhisler konulurken kullanılan mikro akışkan cihazlarda, biyomoleküllerin verimli bir şekilde izolasyonu çok önemlidir. İzolasyon

verimi, tanecik yakalama veriminin ve bağlanma veriminin bir fonksiyonu olarak tanımlanmaktadır. Açıklamak gerekirse, yakalama verimi taneciklerin toplayıcı tarafından yakalanmasının, bağlanma verimi ise yakalanan bir taneciğin bağlanma ihtimalinin bir fonksiyonu olarak tanımlanmaktadır. Bağlanma veriminin önemi aşikar olduğundan bu tez kapsamında yakalama verimi üzerinde durulmuştur.

Biyolojik taneciklerin yakalanması, hava filtreleri ve deniz ekolojisi gibi bilim dallarında tanecik yakalanması üzerinde çalışılmaktadır. Direkt yakalama, difüzyon, atalet kuvvetleriyle yakalama ve yer çekimi kuvvetleri yardımıyla yakalama yöntemleri klasik olarak kullanılan yöntemlerdir. Bunlara ek olarak tanecik katı yüzeye yakın olduğunda etkili olan çeşitli fiziksel etkiler vardır. Direkt yakalama mekanizması akım çizgisi kinematiğinin bir sonucudur. Akım çizgisinin toplayıcıya olan mesafesi taneciğin yarıçapından az olduğunda, akım çizgisini takip eden tanecik toplayıcıya ulaşacaktır. Yakalama verimindeki en önemli faktör direkt yakalamadır. Diğer faktörlerin yakalama verimi üzerindeki etkisi ihmal edilebilir düzeydedir.

Mikro akışkan cihazlarında silikon, cam ya da polimer malzemeler yaygın olarak kullanılmaktadır. Ancak bu tip cihazların kullanımında çeşitli sınırlamalar bulunmaktadır. Örneğin mikron altı parçacıklarda yakalama verimi oldukça düşüktür ve çeşitli parçacıklar için bunun gibi sınırlamalar bulunmaktadır. Ayrıca katı direkler kullanılan bir postta sıvılar için yakalama verimi de oldukça düşüktür. Verimin düşük olmasının iki ana nedeni vardır. Birincisi yığın akış etkisi ikincisi ise yakın yüzey etkisidir.

Bu ve benzeri sorunların önüne geçebilmek için mikro akışkan cihazlarda gözenekli malzemeler kullanılmaktadır. Gözenekli malzemeler katı bir matris ve bunun içerisindeki boşluklu bir yapı olarak tanımlanabilir. Katı bir toplayıcıya göre gözenekli bir toplayıcının yakalama veriminin arttırılması için iki mekanizma önerilir. Birincisi gözenekli toplayıcının şekil değiştirebilme kabiliyeti sayesinde akış alanındaki değişmedir. Bu özellik daha çok taneciğin toplayıcıya gelmesini sağlamakta ve daha çok yakalama sağlamaktadır. İkincisi ise gözenekli bir toplayıcı kullanılması durumunda hidrodinamik direncin azalmasıdır.

Yakalama verimi incelenirken katı ve gözenekli malzemeler dikdörtgen bir kanal içindeki dairesel direkler kullanılan bir model kullanılmıştır. Analizler gözenekli malzemelerin kullanılmasının yakalama verimini arttırdığını göstermiştir. Bundan sonraki analizler yakalama verimini etkileyen parametreler üzerine yoğunlaşmıştır. Bu

parametreler gözenekli malzemenin cinsi, direklerin şekli, değişik direk dizileri ve direk dizilerini etkileyen geometrik parametreler olarak sınıflandırılabilir

Modeller sonlu elemanlar yöntemi kullanılarak COMSOL yazılımı yardımıyla nümerik olarak çözülmüştür. Akışa hakim denklemler süreklilik denklemi ve 2 boyutlu Navier Stokes denklemleridir. Tamamen gözenekli bir yapı içerisindeki akışlar için Darcy Yasası uygulanabilir. Ancak gözeneksiz ve gözenekli ortamlar beraber olduğunda Darcy Yasası doğru sonuç vermez. Buna benzer problemlerin çözümünde Darcy Yasasının Brinkman tarafından yapılan modifikasyonu genel olarak kullanılmaktadır. Su ve kan gibi iki ayrı sıkıştırılamaz akışkan için çeşitli modeller ve çeşitli tanecikler için denklemler çözülmüştür. Akışımız düşük Reynolds sayılı laminer akıştır ve kararlı haldedir.

Sonuçlar gözenekli malzemelerin kullanılmasıyla yakalama veriminin büyük ölçüde iyileştirilebileceğini göstermektedir. Ayrıca altıgen veya kare kesitli direk kullanılması yakalama verimini arttırmaktadır. Ayrıca akışkan olarak kan kullanılmasının, suyla kıyaslandığında yakalama verimini önemli ölçüde arttırdığı gözlenmiştir.

1. INTRODUCTION

Investigation of the factors causing disease is the primary aim of basic researches in the field of bioparticle separation and clinical diagnostics. In this respect, isolation of cells or biomolecules from more complex samples such as blood, sputum, saliva, etc. is required. These bioparticles such as viruses, bacteria, and cells have different sizes with the various orders of magnitude. Unfortunately, there are some limitations for these studies when the target bioparticles in the samples exist in very small quantities. For instance, in the cases of antigen-specific T-cells, circulating tumor cells (CTCs), or HIV viral particles for monitoring immune responses, cancer and AIDS progression, respectively [1].

Furthermore, for many applications in the field of bioparticle separation, efficient isolation of bioparticles is extremely important. Isolation efficiency depends on two factors including the interception efficiency, and the binding efficiency. To clarify, the interception efficiency is the fraction of particles in a flow that are intercepted by a collector, and the binding efficiency is the possibility of binding of the intercepted particles to the surface of a collector [2]. It is noteworthy that because there is no evidence to suggest the measurement of the binding efficiency value, this thesis focuses on interception efficiency.

Solid materials such as polymers, glass or silicon are used for constructing most of the microfluidic devices that are designed for particle separation. However, there are some restrictions for this type of devices. For example, low efficiency of particle capturing, limited function in isolation of sub-micron particles, and limitations in the application for various particle types. Meanwhile, for suspended particles in a liquid, the isolation efficiency of a solid surface is very low. The two reasons causing this are 1) a bulk flow effect (i.e. no-slip boundary condition at solid surfaces causes the flow stagnation) 2) a near-surface effect (i.e. because of the hydrodynamic resistance when a particle approaches a solid surface).

The stated restrictions could be resolved by utilization of porous materials such as porous membranes, monolithic porous plugs, and Vertically Aligned Carbon

Nanotubes (VACNTs). While the porous membranes and the monolithic porous plugs can not address all of the limitations due to the restricted structural properties; however, vertically aligned carbon nanotubes are new porous materials, which is used in microfluidic devices to improve the isolation of bioparticles [2].

One of the microfluidic devices that is used for isolation of bioparticles, consists of a rectangular microchannel in which micro-pillar (i.e. micro posts) arrays are located in the vertical direction with the height equal to the channel height. The materials used for fabrication of this bioseparation device can be a solid or a porous material. Figure 1.1 illustrates the capturing of bioparticles of two size orders by using functionalized (i.e. coated with a chemical material) nanoporous collectors. Figure 1.1a shows the comparison of the isolation of 10-µm-size CD4 T-cells that are fluorescently labeled on a collector of identical geometry, while Figure 1.1b is the illustration of 1-µm-size Streptococcus pneumoniae (i.e. a bacteria type) on nanoporous and solid post arrays with identical geometries [1]

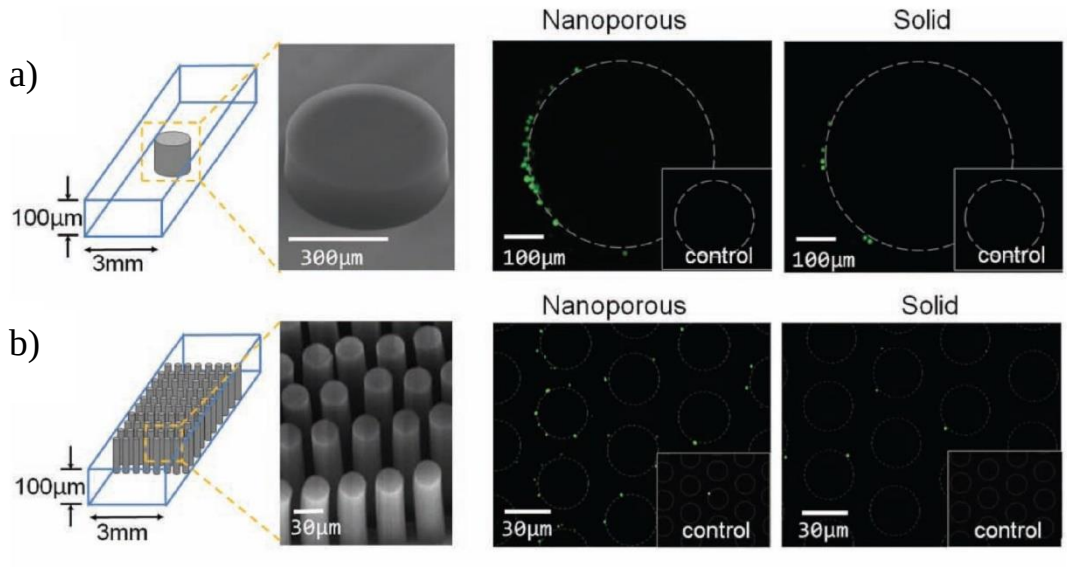

Figure 1.1 : Comparison of the capturing of bioparticles with nanoporous and solid collectors a) a single post b) post arrays. Inset boxes illustrate isolation on non-functionalized control devices [1].

Figure 1.2 emphasizes the comparison of a post made from nanoporous CNT forest and a solid post made from polydimethylsiloxane (PDMS) with the same geometry. One of the advantages of the nanoporous micro-patterned posts is that they are permeable to nanometer-scale particle flow [1]

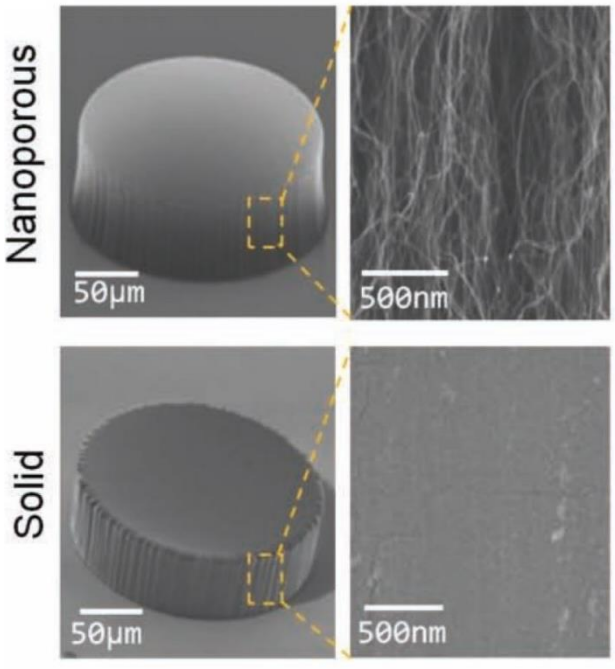

Figure 1.2 : Comparison of a nanoporous and a solid post [1].

Due to the substantial impact of the application of porous materials, investigation of fluid flow inside the medium is necessary. A brief review of the studies about porous media has been presented as follows.

1.1 Literature Review

1.1.1 Background of studies in porous media

The flow of viscous fluid past porous structures is important in different areas of science and technology. It has various applications in chemical engineering [3], especially in porous reactors [4], filtration, and sedimentation [5, 6], also for biomedical studies, where microfluidic devices are used for purification of DNA, or separation of bioparticles [2]. In some of the microfluidic applications, flow inside a microchannel should pass through a porous collector. The surface of these collectors usually is coated with chemical binding moieties (in chemistry moiety means a part or functional group of a molecule). These collectors are designed for serving as a very sensitive detector for biomarkers (a measurable substance in an organism whose presence is indicative of some phenomenon such as disease, infection, or environmental exposure). By utilizing a porous structure, the interaction between the surface of the collector and the fluid (i.e. usually blood or sputum), can highly be improved. While, this improvement is achieved by to factors. 1) By enabling a larger

surface area to volume ratio, and 2) by reducing the influence of hydrodynamic resistance, which is a consequence of the mass transfer boundary layer of a solid impermeable surface. In other words, a boundary layer that is formed near to the solid surface prevents suspended bioparticles from approaching the surface.

Typically, a porous element can be produced from a solid of which, there are interconnected pores or an aggregation of fibers or particles. To describe the motion of fluid inside a porous media, Darcy's law is used. However, for explaining the fluid motion that is inside porous and free media region, other issues such as the interaction between the two regions should be considered. In the literature, there is an analytical method for explaining this interaction, which is the matched asymptotic expansions technique. This technique couples the flow in the two regions namely the Stokes flow in the free media region, and the Darcy flow inside the porous media [7].

The techniques like the mentioned one, are restricted to the flows of low Reynolds number. For investigations that include wide range of Reynolds number, numerical methods are preferred. In this work, the numerical models are utilized to calculate interception efficiency of various cases.

Interception efficiency is defined as the fraction of the span of the upstream streamlines that finally pass the collector with a distance less than one particle radius (on both sides), to the collector diameter. Interception efficiency plays a major role in filtration, and the applications that are designed for particle isolation [8], Meanwhile, the isolation of the particles from a fluid is through the direct interception, inertial impaction, diffusion, and gravitational sedimentation.

Moreover, in the literature, there is another definition for the interception efficiency of flow. According to the definition, the interception efficiency corresponds to the permeation velocity factor. To explain, this factor is the fraction of apparent (or superficial) velocity in the porous region to the velocity of the free media region [6]. The importance of the permeation velocity is in the studies of the transport phenomena through the porous region. For instance, the application of the permeation velocity can be in the estimation of the transport rate by convection, for determining the residence time of a reactant in permeable catalysts, or the systems that include a free media region and a porous structure.

In a recent study of Shahsavari et al. [9] different physical parameters' effect in a laminar flow on a porous cylinder that is confined between two-dimensional parallel plates have been investigated in the steady state. Parameters such as the fluid viscosity, permeability of the porous cylinder, dimensions of the channel on the rate of flow permeation, and flow rate were analyzed.

A theoretical investigation of flow over a permeable cylinder was first performed by Shi and Braden [10]. They studied creeping flow over an unbounded porous cylinder with a circular cross section by utilizing the method of matched asymptotic expansion. By solving the stream function, an analytical expression based on the dimensionless permeability was given for the drag coefficient.

Singh and Gupta [7] employed a similar technique to find the solution of flow over a porous cylinder for various permeabilities. The solution was obtained for a low Reynolds flow in the center region and the outer area.

Effect of permeability on the vorticity pattern and streamlines and drag coefficient in flow over a porous cylinder was studied numerically by Bhattacharyya et al. [11] by utilizing a FEM (i.e. Finite Volume Method). In their investigations, Reynolds number changed between 1 and 40, which was determined based on the diameter of the cylinder.

Yu et al. [12] used a similar method to numerically investigate the viscous flow inside and outside of a porous cylinder in the steady state. Moreover, the influences of the permeability ratio and the inertia of the fluid for a flow with Reynolds number less than 40 were studied to observe the recirculating wake phenomenon and the flow pattern. In addition, the critical Reynolds number was determined based on the Darcy number for beginning of the wake.

Most of the stated studies have considered the flow past a circular post structure. However, the focus of this work is on the investigating the flow over various cross sections and different configuration, which will be discussed in the following chapters.

1.1.2 Background of microfluidic devices used for particle separation

According to Figure 1.3 that shows the size and usual concentration of bioparticles existing in the human blood, Microelectromechanical Systems (MEMS) (specially microfluidics) are utilized for separation of micron size bioparticles. However, for

separation of smaller nano size bioparticles, Nanoelectromechanical Systems (NEMS) is used, which are made of nanoporous materials or nano-fabricated channels.

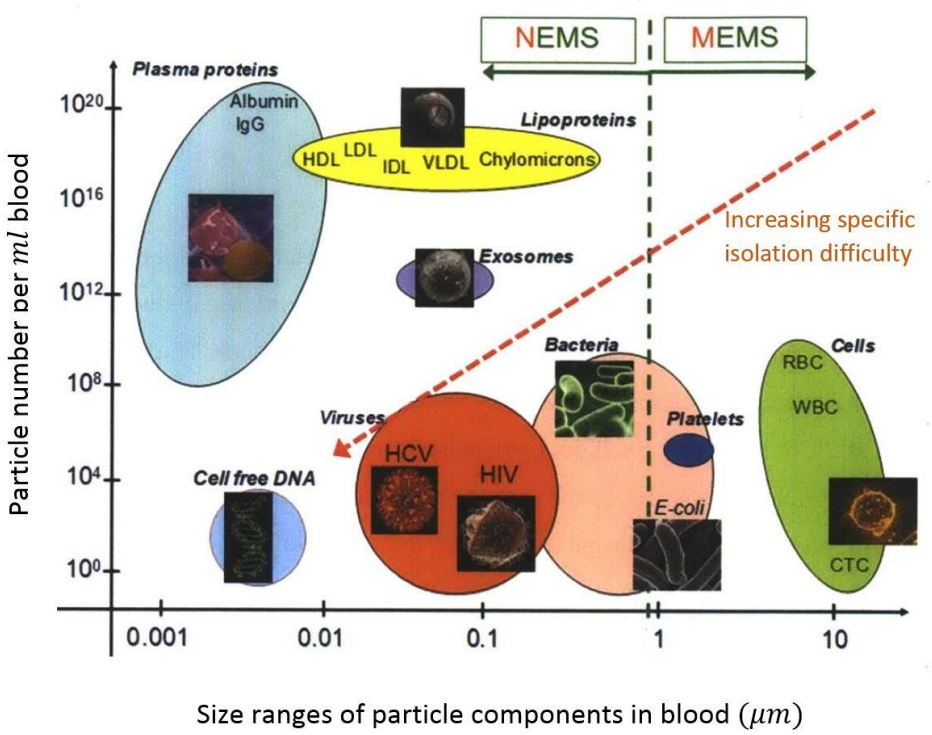

Figure 1.3 : Size and typical concentration of bioparticles present in the blood [13].

Application of microfluidics as an essential tool in analysis and research in biological fields is increasing due to the advantages that it offers in bioparticle separation. Moreover, the advances in the field of bioseparation are one of the necessary outcomes of the benefits provided by microfluidics. The advantages such as lower cost, smaller sample amount, shorter separation duration, understandable fluid dynamics, and disposable devices. Currently, there are various types of microfluidic systems; however, they can be classified into two main groups: 1) Physical properties based platforms in microfluidic separation, and 2) Specific biomolecular recognition based platforms in microfluidic separation [13].

1.1.2.1 Separation platforms based on Physical properties

Microfluidic channels and features can be designed for the application in wide range of bioparticles such as mammalian cells, yeast particles, and even bacteria cells. Physical separation methods make it possible to perform high-level accuracy manipulation that would be hard for macro-scale methods. It should be noticed that

between physical separation methods, inertial focusing and deterministic hydrodynamics are flow-based methods. Brief descriptions of the methods are as follows:

Filtration using patterned solid substrates: For the filtration, porous membranes are usually used in microfluidics. However, their integration into microfluidic devices is unwieldy. While, there are some limitations to this technique including the limits of being functional for the particular size range of bioparticles, limits in filtration area (due to the cross sectional area of the channel), and restrictions to specific geometry (which is restricted to rectangular slits).

Inertial focusing method: In this type of microfluidic devices, inertial forces are used for continuous separation of bioparticles. In addition, the separation of bioparticles can be based on shape and size. In contrast to most of the microfluidic devices, the devices using inertial focusing operate on high flow rate with high output. For instance spiral channels by Bhagat et al. [14], asymmetric curved channels by Dicarlo et al. [15] (Figure 1.4), and spiral channels by Russom et al. [16].

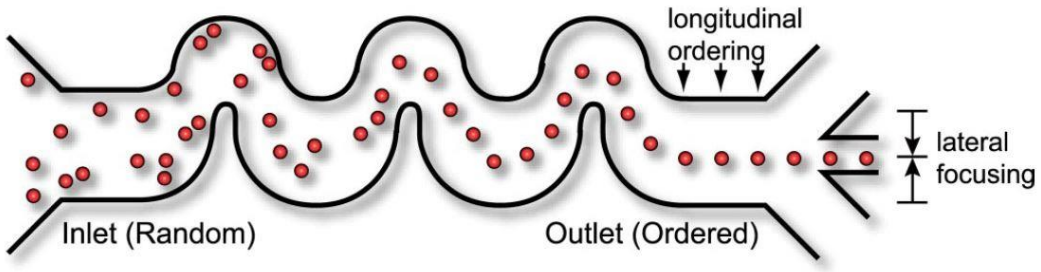

Figure 1.4 : Schematic of a channel of asymmetrically curved inertial focusing [15].

Deterministic hydrodynamics method: Similar to most of the microfluidic devices, in which flow regime typically is laminar, the flow in deterministic hydrodynamics is a low Reynolds number flow [17]. In this method, deterministically sorting of bioparticles is done by asymmetrical bifurcation of laminar flow around obstacles. Application of this technique is for fractionating of micron-sized particles such as bacteria and cells; also, it is known as “bumping” technique [18]. Figure 1.5 illustrates a schematic experiment of this method.

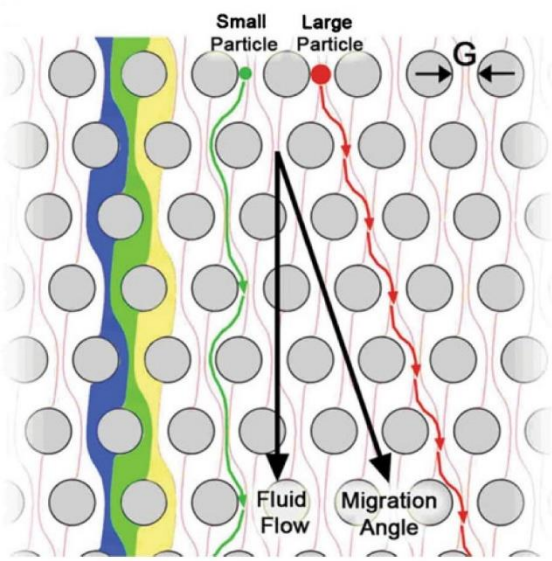

Figure 1.5 : Schematic illustration of particle separation by deterministic hydrodynamics [17].

Dielectrophoresis (DEP) cytometer: Flow cytometry is a laser- or impedance-based, platforms that are used in cell counting, cell sorting, etc. by suspending cells in a fluid flow and passing them by an electronic detection device. By placing a dielectric particle in a non-uniform electric field, a force is imposed on the particle by the uneven field because of the polarization. As an example, Figure 1.6 shows a microfluidic cytometer that uses DEP to trap bioparticles in a fluid flow [19].

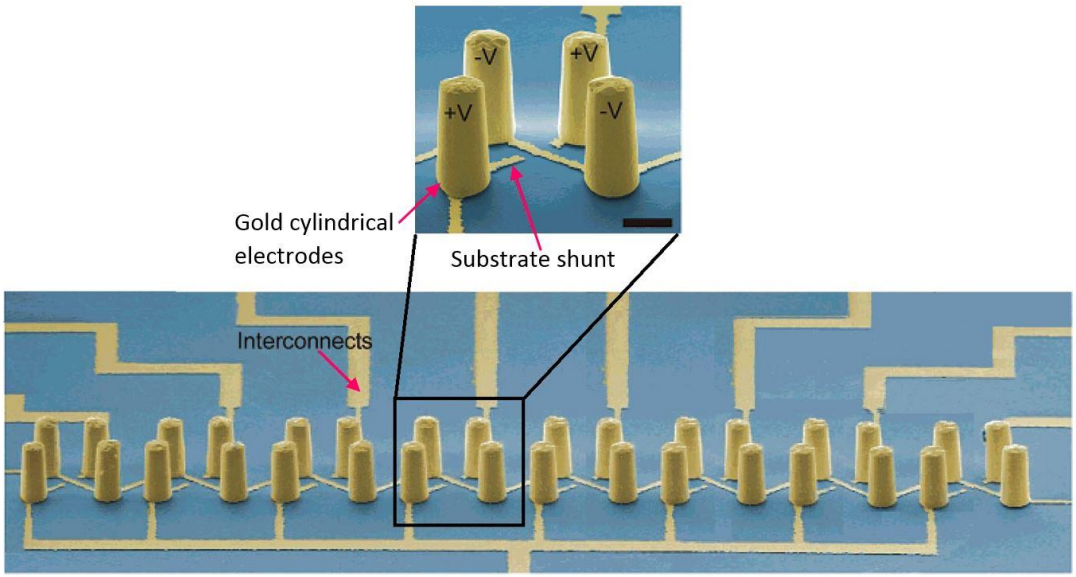

Figure 1.6 : A microfluidic DEP cytometer; SEM (scanning electron micrograph) of a completed 1×8 trap array [19].

Optical manipulation techniques: Optical tweezer is the most frequent example of optical traps. They consist of laser beams, which are tightly focused in a way that can confine dielectric particles in three dimensions. The advantages such as high precision, contamination free, and non-contact nature, make them attractive tools in many microfluidic applications [20].

Acoustic trapping technique: In microfluidics, this technique is utilized to trap cells or micro bioparticles in a non-contacting manner. Figure 1.7 shows a typical setup, which creates acoustic standing waves. Stationary pressure gradients that is generated by ultrasonic standing waves exert forces on particles in a liquid medium, and the particles can be confined in nodal positions. The application of acoustic traps can be in the enhancement of bead-based immunoassays, sample enrichment, and 2-D cell arrays [21].

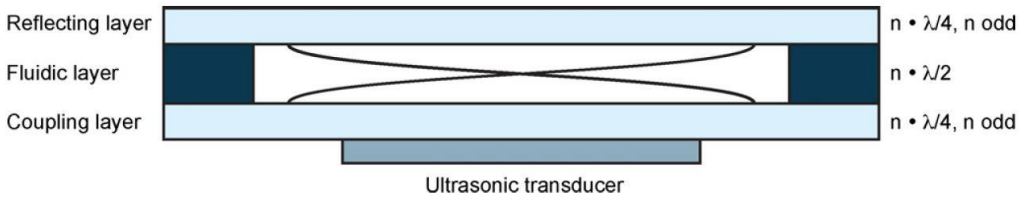

Figure 1.7 : Schematic of a multilayer resonant structure [22].

1.1.2.2 Separation platforms based on specific biomolecular recognition

The methods of specific separation of bioparticle are similarly taken from macro scale separation techniques. Both of the microfluidic MACS and FACS are liquid phase techniques and need labeling of the sample. However, microfluidic affinity chromatography does not require labeling, and it is solid phase.

Functionalized magnetic beads: In general, the methods that adapt magnetic activated cell sorting (MACS) to microfluidics can be divided into two groups, which are based on the source of the magnetic field. The first group is active traps, and use electrical power to generate magnetic fields through on-chip electromagnets (Figure 1.8 a) [23]. However, the other group is the passive traps in which the magnetic field is usually generated by a permanent magnet located off-chip, with on-chip iron or nickel elements. For instance, in Figure 1.8 b, an external magnetic field is shown, in which patterned nickel strips guide magnetic beads in one direction, whereas non-magnetic beads move in the direction of the flow [23].

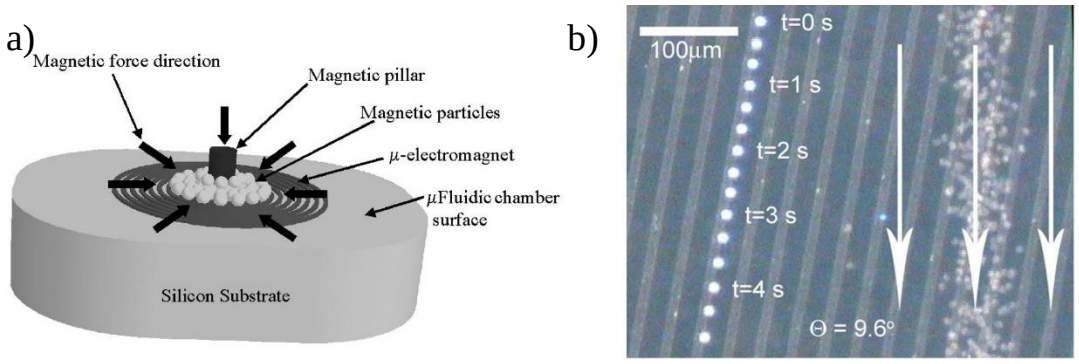

Figure 1.8 : a) Active magnetic separation device. b) Passive magnetic separation device [23].

Microfluidic flow cytometry: As stated, one type of flow cytometry is a laser-based microfluidic device. For example, Figure 1.9 shows a high-throughput microfluidic device, which is employed to cells sorting. To explain, fluorescently identified cells are deflected to the target output channel by an optical force, which is generated by a focused laser. Although the flow components can be successfully miniaturized by this method, the need for large and expensive optics off-chip for fluorescent detection remains a major obstacle for extensive implementation of this technique [24].

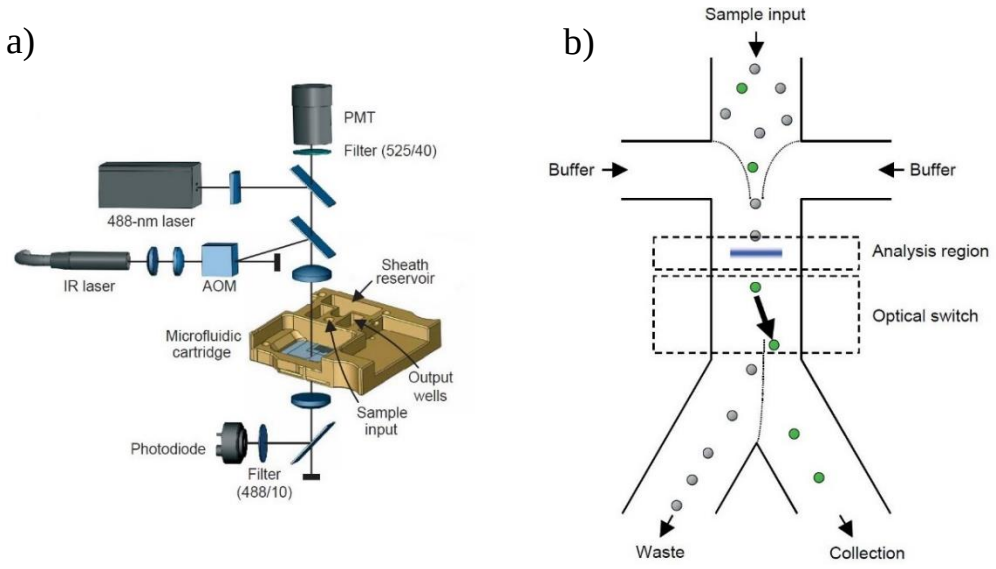

Figure 1.9 : a) Schematic of the optical cell sorter instrument. b) The layout of the device [24].

Microfluidic affinity chromatography: Affinity chromatography is a technique of separating biochemical mixtures based on a highly specific interaction such as that between antigen and antibody, enzyme and substrate, or receptor and ligand [25]. This technique is an appropriate choice for mammalian cells because of its clear fluid dynamics and the micron-range size scale of devices. Moreover, in comparison with

microscale FACS and MACS methods, microfluidic affinity chromatography has some advantages such as no necessity of pre-mixing the sample with labels, no need for large off-chip parts, and higher reliability of results due to the predictable fluid dynamics [26]. Figures 1.10a-1.10c show a microfluidic device for isolating CD4+ T-cells directly from whole blood; And, Figure 1.11 is the example of the device utilized for affinity capture of circulating tumor cells (CTCs).

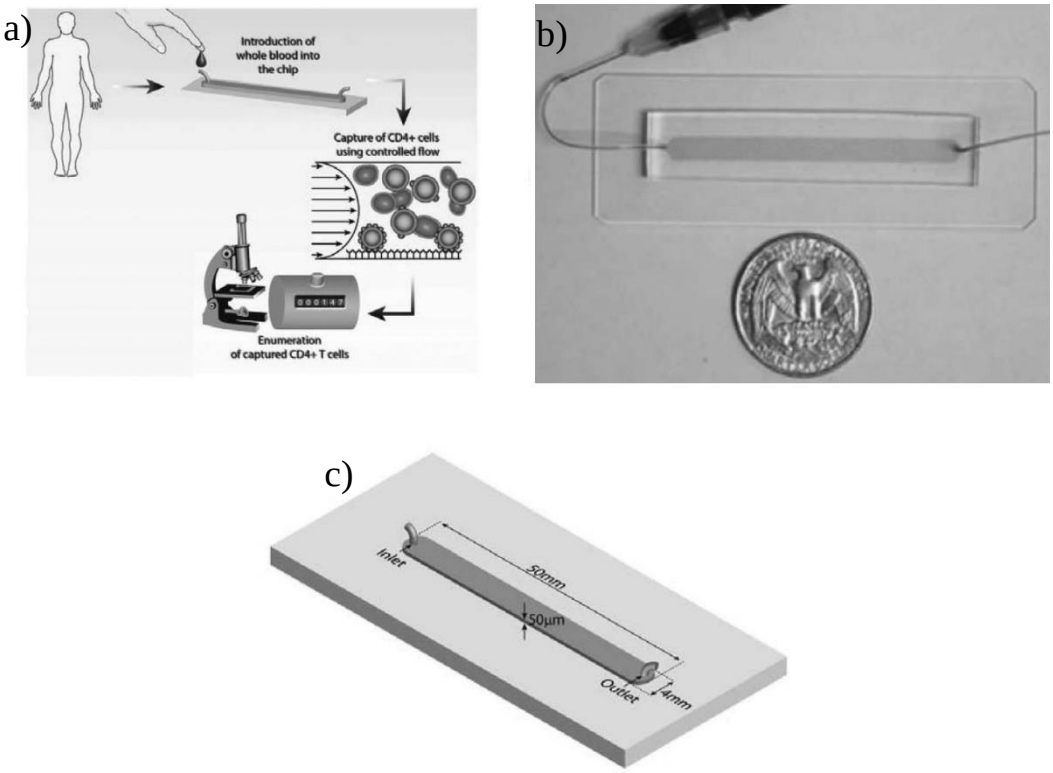

Figure 1.10 : a) Schematic depiction of a CD4 counting device. b) Picture of a linear cell-counting device. c) Geometry of the device [27].

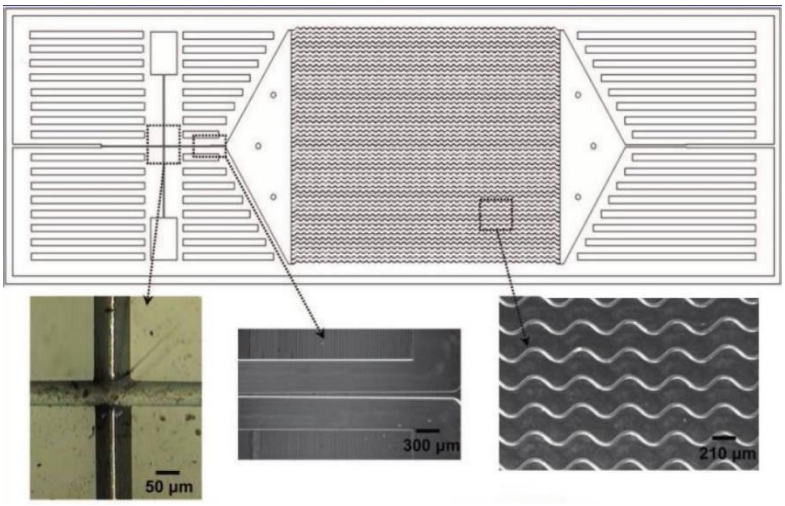

Figure 1.11 : Schematics of a device used for capturing CTCs [28].

1.2 Research Objectives

The primary purpose of this thesis is to investigate the effect of various parameters on the interception efficiency of a post inside a rectangular channel. The studied parameters are as follows.

- Impact of the different materials of the post.
- Influence of the shape of the post.
- Effect of the configuration of the posts.
- Effect of the geometrical parameters between posts.

The obtained results are compared in order to find the optimum cases in which higher interception efficiency could be achieved.

2. GOVERNING EQUATIONS AND THEORETICAL INVESTIGATIONS

The involved equations and various factors that affect the particle interception have been discussed as follows:

2.1 Navier-Stokes Equations

The well-known Navier-Stokes equation is the governing equation for the motion of fluids, which represents the conservation of momentum. In the case of an incompressible fluid, it can be written as equation (2.1) [29]:

$$\frac{\partial \mathbf{v}}{\partial t} + \mathbf{v}.(\nabla \mathbf{v}) = -\frac{1}{\rho}\nabla P + \frac{\mu}{\rho}\nabla^2 \mathbf{v} \tag{2.1}$$

Where, $\mathbf{v} = \mathbf{v}$(u,v) is the fluid velocity (m/s), P is the fluid pressure (Pa), ρ is the fluid density (kg/m^3), and μ is the fluid dynamic viscosity $(Pa.s)$.

For the steady state flow, it can be written as equation (2.2):

$$\mathbf{v}.(\nabla \mathbf{v}) = -\frac{1}{\rho}\nabla P + \frac{\mu}{\rho}\nabla^2 \mathbf{v} \tag{2.2}$$

In addition, the continuity equation represents the conservation of mass, and in the case of an incompressible fluid in the steady state flow, it is as the equation (2.3):

$$(\nabla.\mathbf{v}) = 0 \tag{2.3}$$

2.2 Darcy's Law

Darcy's law gives a fundamental equation to describe a flow inside a porous medium. By neglecting body forces such as gravity, in three dimensions it is written as equation (2.4) [30]:

$$\mathbf{v} = \mu^{-1}\boldsymbol{\kappa} \cdot \nabla P \tag{2.4}$$

Where, $\mathbf{v} = \mathbf{v}$(u, v) is the volume-averaged velocity vector (m/s), P is the pressure (Pa), μ is the dynamic viscosity $(Pa.s)$, and the permeability $\boldsymbol{\kappa}$ is in general, a second-order tensor. If the medium is isotropic, the permeability is a scalar; meaning that, the porous matrix is incompressible. By simplifying equation (2.4) it becomes (equation (2.5)):

$$\nabla P = -\frac{\mu}{\kappa}\mathbf{v} \tag{2.5}$$

For natural materials values of κ have a wide range. The coefficient κ called the *intrinsic permeability or specific permeability* of the medium, and its dimension is $(length)^2$. For the case of a single phase flow, it is abbreviated to permeability. Nature of the fluid has no effect on κ but it is dependent on the medium geometry.

In dimensionless form, equation (2.5) can be written as equation (2.6) [13]:

$$\mathbf{v}' = -\frac{\kappa}{a^2}\nabla P' \tag{2.6}$$

Where, $\mathbf{v}' = \mathbf{v} \,/\, U$ is the non-dimensional velocity, U is the far field uniform stream velocity, a is the characteristic length, and $P' = aP/\mu U$ is the non-dimensional mean pressure. The characteristic length is dependent on the geometry. For cylindrical geometries, the characteristic length is the diameter.

The dimensionless Darcy number, *Da*, can be defined by the equation (2.7). This dimensionless number relates permeability κ and characteristic length a of porous material, and it indicates the accessibility of the fluid inside the porous medium. Furthermore, it is the fundamental parameter in the comparison between the porous structures. So, equation (2.6) may be written as (equation (2.7)):

$$\mathbf{v}' = -\boldsymbol{Da}\nabla P' \tag{2.7}$$

2.3 Brinkman's Equation

Brinkman's equation (equation (2.8)) is commonly considered as an alternative for Darcy's equation. Application of it is for the flow regimes that are a combination of free and porous media [30].

$$\nabla P = -\frac{\mu}{\kappa}\mathbf{v} + \tilde{\mu}\nabla^2\mathbf{v} \tag{2.8}$$

Where, P is the pressure (Pa), μ is the dynamic viscosity $(Pa.s)$, κ is the permeability (m^2), $\mathbf{v}$ is the volume-averaged velocity vector (ms^{-1}), $\tilde{\mu}$ is known as the effective viscosity, and is given by the equation (2.9):

$$\frac{\tilde{\mu}}{\mu} = \frac{1}{\varphi} \tag{2.9}$$

Where, φ is the porosity of the porous medium.

The advantage of Brinkman's equation is that it matches the boundary conditions at the interface between free and porous media.

In analyzing fluid flow in a combination of free and porous media, the assumptions for boundary conditions at the interface of fluid and porous structure is critical. According to the conservation of mass, mass flux through the boundary should be continuous. Moreover, at the boundary, the pressure should be continuous. It should be noted that in the interface of a liquid and porous structure, the no-slip condition is not applicable.

It is important to mention that there is another common phenomenon that is called jump condition, in the combination of the porous and free media flow. This condition is proposed by Ochoa-Tapia and Whitaker [31], and it arises when the momentum transfer condition is applied at the boundary of these media. In addition, the jump condition is produced to join the Stokes and Brinkman's equations together, and it occurs in the stress but not in the velocity.

Partha [32] has investigated the influence of stress jump and he found that when the Darcy number is higher than 10^{-2}, (i.e. $Da > 10^{-2}$), the effect of stress jump becomes vital. However, below this limit, its influence can be neglected.

It should be noted that the range of Darcy number within this work remains under the critical value. Thus, the value of stress jump is assumed to be negligible.

2.4 Theoretical Issues of Particle Interception

Interception of particles is studied in various realms of science such as biological particle capturing, air filtration, marine ecology, etc. The four principal mechanisms

that are known as the classical mechanisms, contribute in particle interception, which are as follows [2]:

- Direct interception
- Diffusion
- Inertial impaction
- Gravitational sedimentation

In the following, detailed explanations of above mechanisms have been presented. It should be mentioned that focus of this work is on investigations of necessary parameters' impact on direct interception efficiency.

Figure 2.1 shows the direct interception mechanism. This mechanism is a result of streamline kinematics. To explain, when a moving particle in a flow locates on a streamline, which finally approaches the post with a distance less than the radius of the particle, it collides to the post and the direct interception occurs.

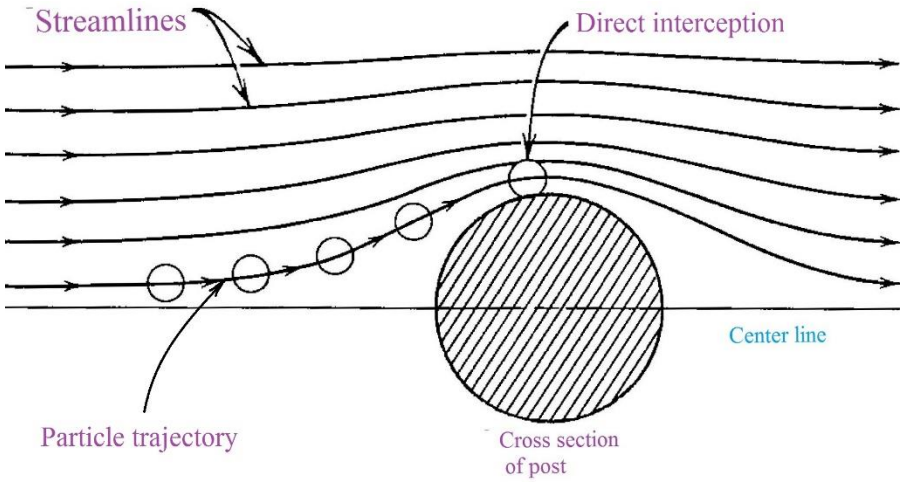

Figure 2.1 : Schematic illustration of direct interception mechanism.

Determining interception efficiency: The direct interception is the most dominant mechanism between others. To understand the direct interception, a simple model of the circular post is illustrated in Figure 2.2. equation (2.10) is used for calculating direct interception efficiency [2]:

$$\eta_i = \frac{b}{d_c} \tag{2.10}$$

Where, b is the span of upstream streamlines that finally pass exactly one particle radius away from the surface of the post (on both sides), and d_c is the collector (or post) diameter. The parameter b is obtained by the exported data of streamlines that are resulted from numerical simulation. To clarify, the thickness b of upstream streamlines is measured by depicting the streamlines that finally pass the post with a distance less than a particle radius.

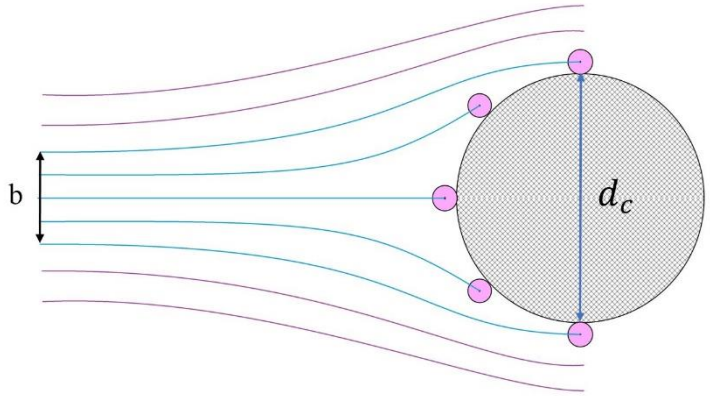

Figure 2.2 : Schematic of a post for the definition of interception efficiency.

In a fluid, the Brownian diffusion is dominant for very small particles (Figure 2.3). The occurrence of this mechanism is due to the random movements of the particle between flow streamlines. Besides, the diffusive activity of a particle can be increased by some factors such as temperature, and the longer staying time of particle near the post, which will lead to increasing the chance of collision of the particle to the post.

The equation (2.11) is given for the efficiency of interception by Brownian diffusion:

$$\eta_{diff} = \frac{3.64 A_F}{Pe^{2/3}} \tag{2.11}$$

Where Pe= L*U*/D is the Peclet number (convection/diffusion), L is the characteristic length, *U* is the average velocity in the channel, and D is the diffusion coefficient which is equal to $kT/6\pi\mu a_p$ (*k* is the Boltzmann constant, *T* is temperature in Kelvin, μ is viscosity, and $a_p$is the particle radius), and equation (2.12) defines the coefficient A_F is [13]:

$$A_F = [2 - \ln\left(\frac{2d_c U}{\nu}\right)]^{-1} \tag{2.12}$$

Where d_c is the collector (post) diameter, U is the average velocity in the channel, and ν is the kinematic viscosity.

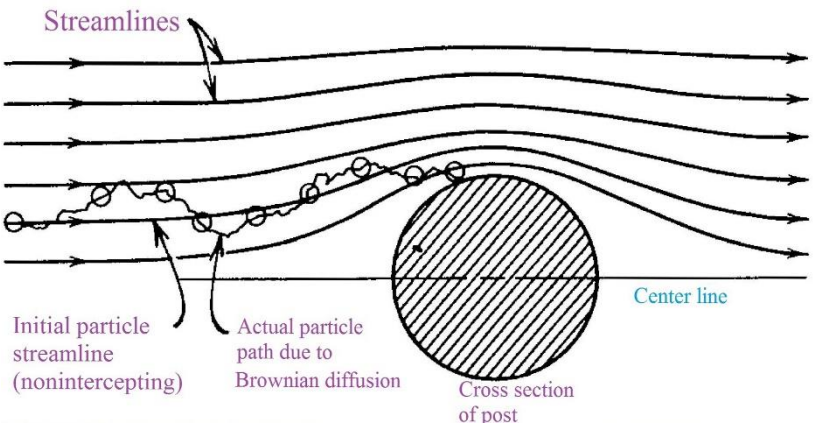

Figure 2.3 : Schematic illustration of Brownian diffusion mechanism.

For particles larger than 1 or 2 μm in diameter, the contribution of diffusion generally is not important [2]. For instance, in the experimental work of Chen et al. [13] the range of Pe number is between 2×10^4 corresponding to 1 μm particle and 50 μm post diameter, and 1×10^7 for particle size of 10 μm and post diameter of 500 μm. For their experimental conditions, the obtained values of η_{diff} for mentioned rang of Peclet number, change between 0.0009 and 0.00003. Therefore, the contribution of diffusion is insignificant for particles larger than 1 μm or 2 μm diameter.

The mechanism of inertial impaction is illustrated in Figure 2.4. It is as a result of the deviation of the particle from flow streamlines and colliding with the post due to its inertia. This mechanism is important for suspended particles in air filtration systems. The Stoke's number (equation (2.13)) shows the effect of the inertial impaction [33]:

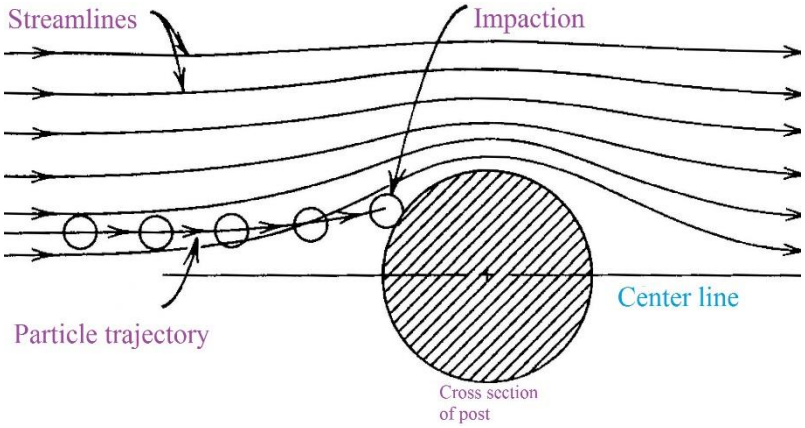

Figure 2.4 : Schematic illustration of inertial impaction mechanism.

$$Stk = \frac{1}{9} Re \left(\frac{d_p}{d_c}\right)^2 (s - 1) \tag{2.13}$$

Where, Re is the Reynolds number, d_p is the particle diameter, d_c is the post diameter, s is the specific gravity (i.e. the ratio of density of a substance to density of water). According to [33], for $Stk < 0.125$ the effect of inertial impaction can be neglected.

Gravitational sedimentation is another contributor for the interception of particles, and it is shown in Figure 2.5. The occurrence of this mechanism is for the cases that posts are horizontally located in the flow, and the particles moving along the streamlines at the top of the posts, can settle on their surface. For the cases that posts' orientation are vertical, the gravitational sedimentation does not happen [34].

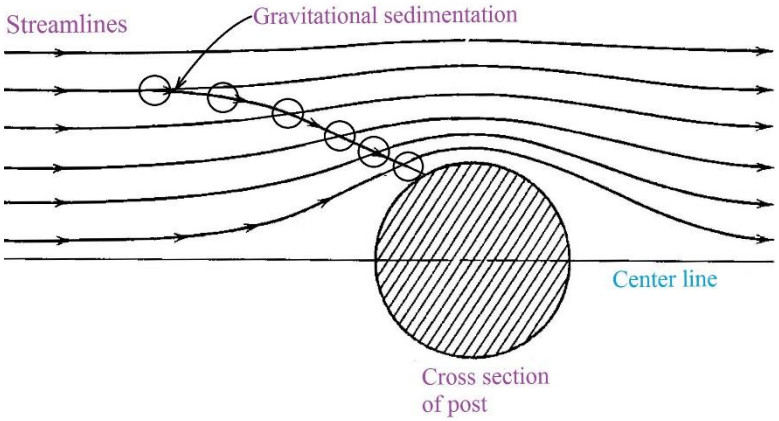

Figure 2.5 : Schematic illustration of gravitational sedimentation.

In addition to the four mechanisms of particle interception, there are other important physical effects imposed by the post surface on a particle when it approaches the post. These surface effects are:

- The hydrodynamic resistance between the particle and post.
- The London forces of molecular attraction.

The hydrodynamic resistance between the particle and solid surface can be described as a resisting force that prevents the particle to approach the surface. In contrast, the London (or van de Waals) force is opposite to the hydrodynamic resistance force, and it causes the particle to be attracted the surface. Also, this force dominates when the distance between the particle and surface reduces to molecular dimensions [2].

Effect of these forces is analyzed by Goren [35] and Spielman [36], and combined effect of them on direct interception efficiency is given by a parameter known as the adhesion coefficient denoted by N_{Ad} equation (2.14):

$$N_{Ad} = \frac{H{d_c}^2}{9\pi\mu{d_p}^4 U A_F} \tag{2.14}$$

Where H is the Hamaker constant, d_c is the collector (post) diameter, μ is the fluid dynamic viscosity, d_p is the particle diameter, U is the average velocity in the channel.

Near-surface hydrodynamic resistance for a solid post has a significant value; so by considering this effect, direct interception efficiency should be adjusted. The modification or adjustment factor is defined as the below ratio (equation (2.15)) [35]:

$$\frac{\eta}{\eta_i} = \frac{\text{adjusted efficiency}}{\text{obtained efficiency by direct interception}} \tag{2.15}$$

The relationship for adjustment factor and the adhesion coefficient is calculated by Goren [35] and is shown in Figure 2.6 below. For the small values of adhesion coefficient, the effect of hydrodynamic resistance is dominant whereas, for large values of it, the London forces have greater influence.

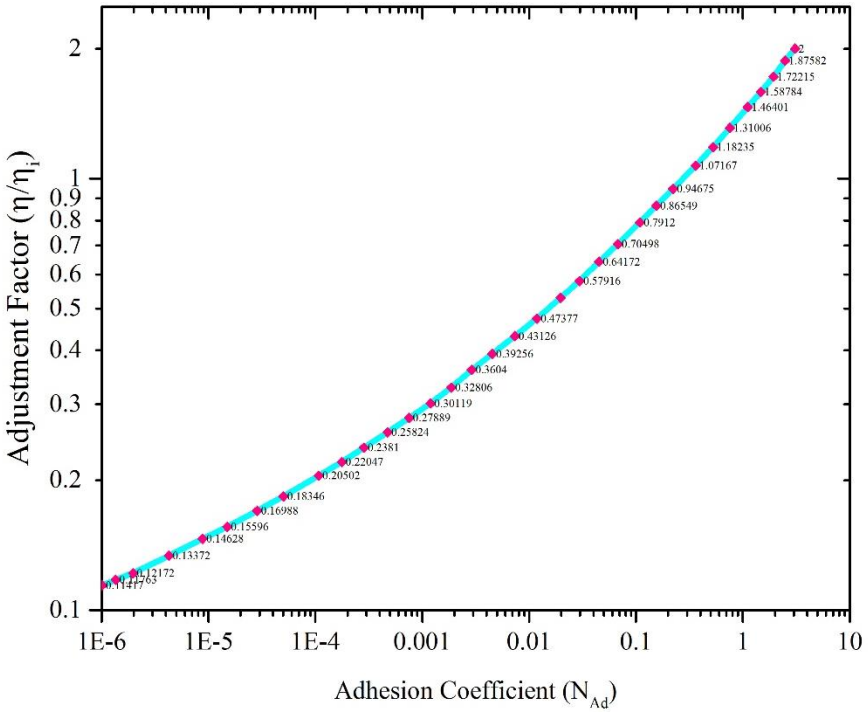

Figure 2.6 : Adjustment factor for interception efficiency based on N_{Ad}. (adapted from [35]).

3. MODEL DESCRIPTION FOR PARAMETRIC STUDIES

Based on the explanations of previous chapters about particle interception and porous media; in this chapter models are developed to investigate the flow field and other essential issues such as streamlines pattern. Models are simulated in COMSOL Multiphysics (v5.2) to obtain corresponding data from 2-D numerical models of the flow field. Derived results have been presented in Chapter 4.

3.1 Model Definition for the Single Circular Solid Post

Figure 3.1 illustrates the schematic model of the single solid post with a circular cross section inside a rectangular channel (i.e. a top view of the channels is shown). Parameters of the geometry are given in Table 3.1.

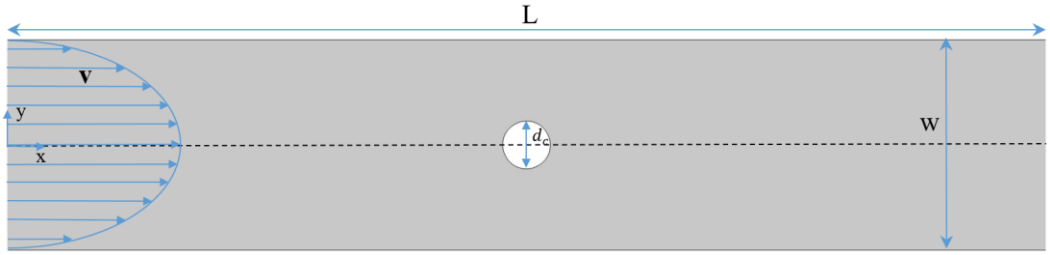

Figure 3.1 : Schematic model of the single solid post with a circular cross section inside a rectangular channel.

Table 3.1 : Geometrical parameters of Figure 3.1.

Parameter	Description
L	Length of the channel
w	Width of the channel
d_c	Diameter

For simulation of the solid post model, Laminar Flow Model has been chosen in COMSOL software. The application of Laminar Flow Model is for computing the velocity and pressure fields for the flow of a single-phase fluid in a laminar flow regime. The governing equations for studied case are the continuity equation (3.1) for the conservation of mass, and the 2-D Navier-Stokes equation (3.2) for the conservation of momentum for an incompressible viscous flow. The analysis is

performed in the steady state. (In Chapter 2, detailed discussions of governing equations are presented).

$$(\nabla . \mathbf{v}) = 0 \tag{3.1}$$

$$\mathbf{v}.(\nabla \mathbf{v}) = -\frac{1}{\rho}\nabla P + \frac{\mu}{\rho}\nabla^2 \mathbf{v} \tag{3.2}$$

Here, **v** denotes the velocity vector; P is the pressure, ρ and μ are the fluid density and dynamic viscosity.

Boundary conditions for a Single Circular Solid Post (B. C. I):
The applied boundary conditions for the solid post model are as follows:

- At the inlet ($x = 0$), the fully developed velocity condition $\mathbf{v} = \frac{3}{2}U[1 - \left(\frac{y}{w/2}\right)^2]$ where, U is the average velocity, is used. This fully developed condition is mapped from the outlet of pre-calculated straight channel at the same width.
- At the walls ($y = \pm w/2$) as well as the surface of the post, no-slip boundary condition (i.e. $\mathbf{v} = 0$) is assumed.
- The boundary condition for the outlet ($x = L$) is zero pressure $P = 0$.

3.2 Model Definition for the Single Circular Porous Post

Similar to the solid post model, Figure 3.2 schematically shows a single porous post with a circular cross section inside a rectangular channel.

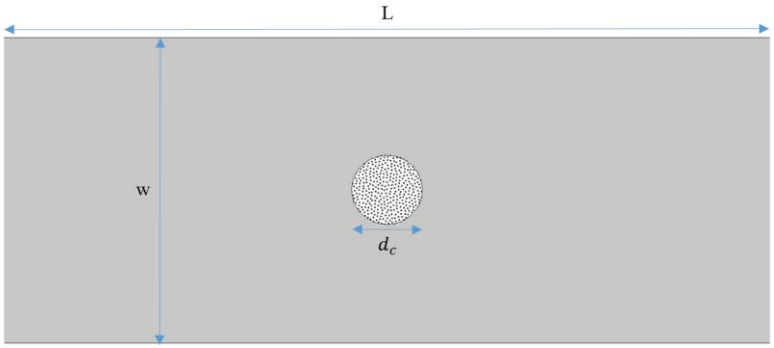

Figure 3.2 : Schematic of a single porous post with a circular cross section inside a rectangular channel.

This model (Figure 3.3) consists of a single circular porous post inside a rectangular channel similar to the solid post model. There are two domains for the models of porous posts, including inside the post (i.e. porous medium that is denoted by p subscript) and the free media domain (i.e. outside, which is denoted by f subscript). Properties of the geometry of the model are delivered in Table 3.2. The aim of investigating this case is to compare interception efficiency of a porous post with a solid post of identical geometries.

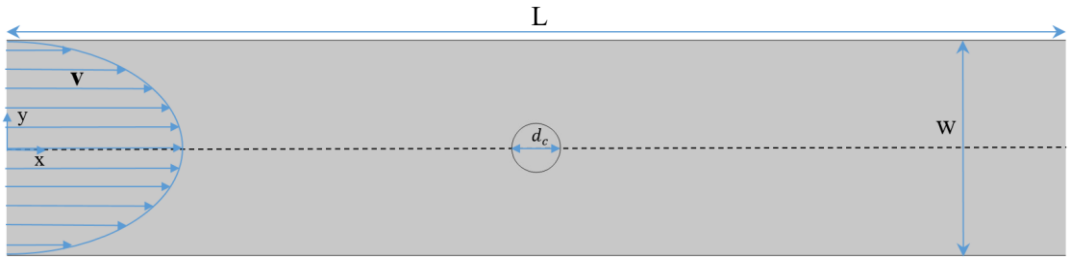

Figure 3.3 : Schematic model of the single circular porous post.

Table 3.2 : Geometrical parameters of Figure 3.3.

Parameter	Description
L	Length of the channel
w	Width of the channel
d_c	Characteristic length

In this thesis, characteristic length of a porous post is defined as the maximum length of the post in different cross sections. For the case of a circular post, characteristic length is equal to its diameter.

For simulation of the porous post model, Brinkman Equation Model has been selected in COMSOL software. Brinkman Equation Model is a sub-branch of Porous Media and Subsurface Flow. This model is used to compute fluid velocity and pressure fields of single-phase flow in porous media in a laminar flow regime. The equations (3.1-3.3) are governing equations for studied case.

$$\nabla P = -\frac{\mu}{\kappa}\mathbf{v} + \tilde{\mu}\nabla^2\mathbf{v} \tag{3.3}$$

- The continuity equation for conservation of mass (equation 3.1) and the 2-D Navier-Stokes equation (equation 3.2) for the free media sub-domain.
- The 2-D Brinkman equation (equation 3.3) for the porous sub-domain.

Which, have been solved numerically for an incompressible viscous flow in the steady state.

Boundary conditions for the Single Circular Porous Post (B. C. II):
The applied boundary conditions for the porous post model are as follows:

- At the inlet ($x = 0$), the fully developed velocity condition $\mathbf{v} = \frac{3}{2}U[1 - \left(\frac{y}{w/2}\right)^2]$ where, U is the average velocity, is used. This fully developed condition is mapped from the outlet of pre-calculated straight channel at the same width.
- At the walls ($y = \pm w/2$), no-slip boundary condition (i.e. $\mathbf{v} = 0$) is assumed.
- The boundary condition for the outlet ($x = L$) is zero pressure $P = 0$.
- Assumptions for the boundary conditions in the interface of the free and porous domains are the continuity in pressure $P_f = P_p$, and velocity $\mathbf{v}_f = \mathbf{v}_p$.
- As it mentioned in section (2.3), in the combination of the porous and free media flow jump condition should be considered. It arises when the momentum transfer condition is applied at the boundary of these media. Also, the jump condition is for joining the Stokes and Brinkman's equations together, and it occurs in the stress. Based on [32] the stress jump is considered as zero since Darcy number remains below the critical value of 0.01.

3.3 Models Definition for Various Shape of the Post

In order to expand the investigations of interception efficiency, models with more complicated post cross sections have been designed. The studied models are a NACA-12 airfoil, truncated hexagon, square, and regular hexagon which are shown in Figure 3.4.

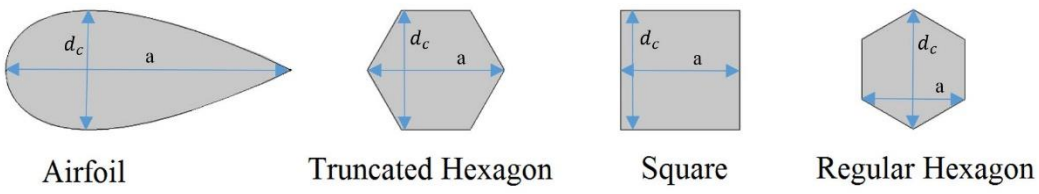

Figure 3.4 : Schematic illustration of different posts cross sections.

The parameters d_c and a, are defined as the width and the characteristic length of a post. The investigations of interception efficiency of the various posts' shapes have been performed for a constant post width.

For all of the following models, the continuity equation (equation 3.1) and the 2-D Navier-Stokes equation (equation 3.2) for the free media region, and the 2-D Brinkman equation (equation 3.3) for the porous region are the governing equations. Additionally, the utilized boundary conditions for these models are as the same as the boundary conditions of the single porous post model introduced previously (B. C. II) (section 3.2).

The model used for the airfoil is NACA 0012 which is as follows (equation (3.4)):

$$y = \pm c \cdot 0.594689181 \cdot \left(0.298222773 \cdot \sqrt{\frac{x}{c}} - 0.127125232 \cdot \frac{x}{c} - 0.357907906 \cdot \left(\frac{x}{c}\right)^2 + 0.291984971 \cdot \left(\frac{x}{c}\right)^3 - 0.105174696 \cdot \left(\frac{x}{c}\right)^4 \right) \quad (3.4)$$

Where, c is the chord of the airfoil. Figure 3.5 schematically illustrates the airfoil post inside a rectangular channel, and the geometrical properties of the model are given in Table 3.3.

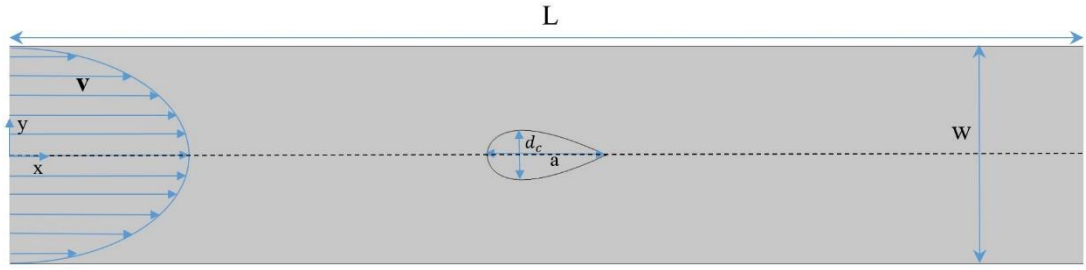

Figure 3.5 : Schematic model of the single porous airfoil post.

Table 3.3 : Values of geometrical parameters of Figure 3.5.

Parameter	Description	Value
L	Length of the channel	20 (mm)
w	Width of the channel	2.2 (mm)
a	Characteristic length of the post (chord of the airfoil)	1200 (μm)
d_c	Width of the post	500 (μm)

The schematic model of the truncated hexagon post inside a rectangular channel is shown in Figure 3.6. While, the geometrical properties of the model are given in Table 3.4.

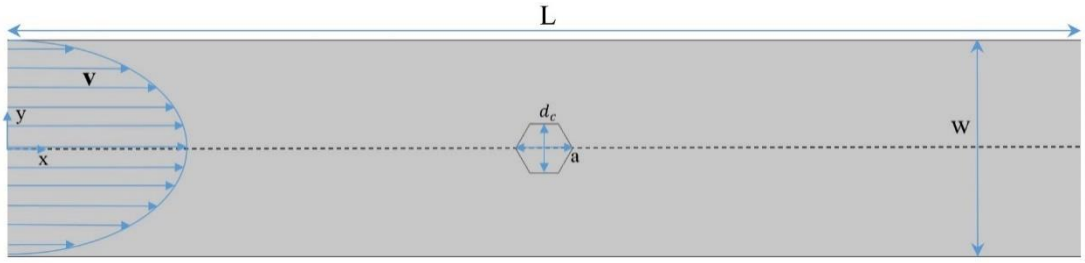

Figure 3.6 : Schematic model of the single porous truncated hexagon post.

Table 3.4 : Values of geometrical parameters of Figure 3.6.

Parameter	Description	Value
L	Length of the channel	20 (mm)
w	Width of the channel	2.2 (mm)
a	Characteristic length of the post	577.35 (μm)
d_c	Width of the post	500 (μm)

Similarly, the model of the square post is schematically illustrated in Figure 3.7, and the geometrical properties of the model are given in Table 3.5.

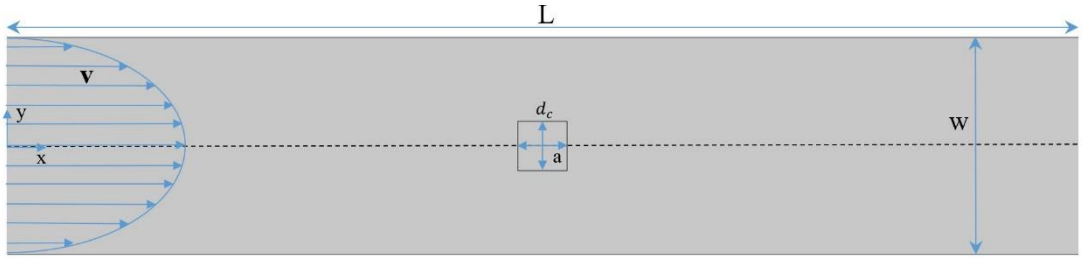

Figure 3.7 : Schematic model of the single porous square post.

Table 3.5 : Values of geometrical parameters of Figure 3.7.

Parameter	Description	Value
L	Length of the channel	20 (mm)
w	Width of the channel	2.2 (mm)
a	Characteristic length of the post	500 (μm)
d_c	Width of the post	500 (μm)

Similar to the previous models, Figure 3.8 is the schematic illustration of the regular hexagon post, and the geometrical properties of the model are given in Table 3.6.

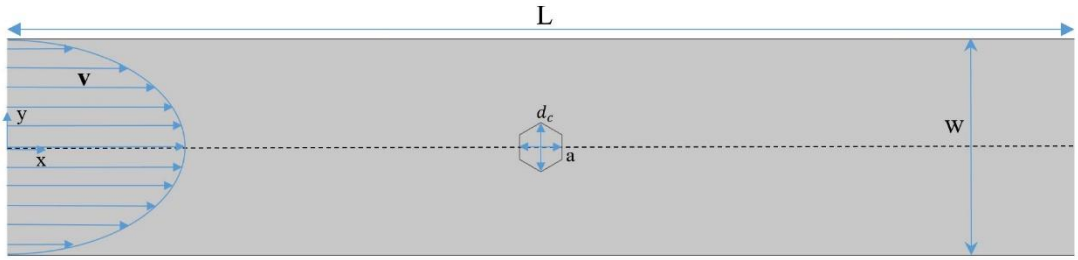

Figure 3.8 : Schematic model of the single porous regular hexagon post.

Table 3.6 : Values of geometrical parameters of Figure 3.8.

Parameter	Description	Value
L	Length of the channel	20 (mm)
w	Width of the channel	2.2 (mm)
a	Characteristic length of the post	433 (μm)
d_c	Width of the post	500 (μm)

3.4 Model Definition for Configuration of the Posts

In microfluidic devices, application of posts array are more common and a single form of a post is rarely used for particle separation. Figure 3.9 shows a microfluidic device consisting micro-pillars, and Figure 3.10 shows the schematic representations of square and equilateral triangle posts array that have been chosen for the simulations. For both of the configurations, the models are designed for various post cross sections. The goal of developing these models is to observe the impact of the proximity of the adjacent posts on the interception efficiency of a single post within the array.

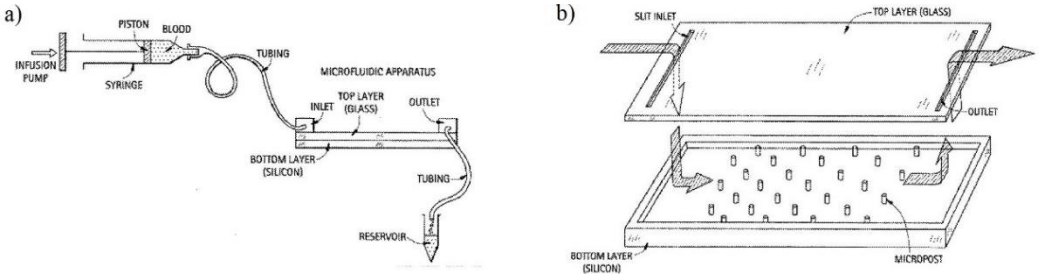

Figure 3.9 : a) A schematic depiction of a cell-binding device. b) an exploded view of a cell-binding device of Figure a [37].

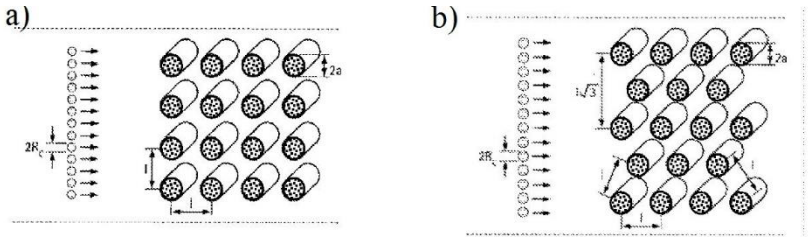

Figure 3.10 : a) A schematic illustration of a square array of circular posts. b) a schematic illustration of an equilateral triangle array of circular posts [37].

Similar to the previous section, for all of the following models, the governing equations are the continuity equation (equation 3.1) and the 2-D Navier-Stokes equations (equation 3.2) for the free media region. Meanwhile, the 2-D Brinkman equation (equation 3.3) used for the porous region. They have been numerically solved in the steady state for incompressible viscous flow. Furthermore, the applied boundary conditions for these models are identical to the boundary conditions of the single porous post model (B. C. II).

Figure 3.11 schematically shows the square and equilateral triangle configurations of the circular posts array, which properties are given in Table 3.7.

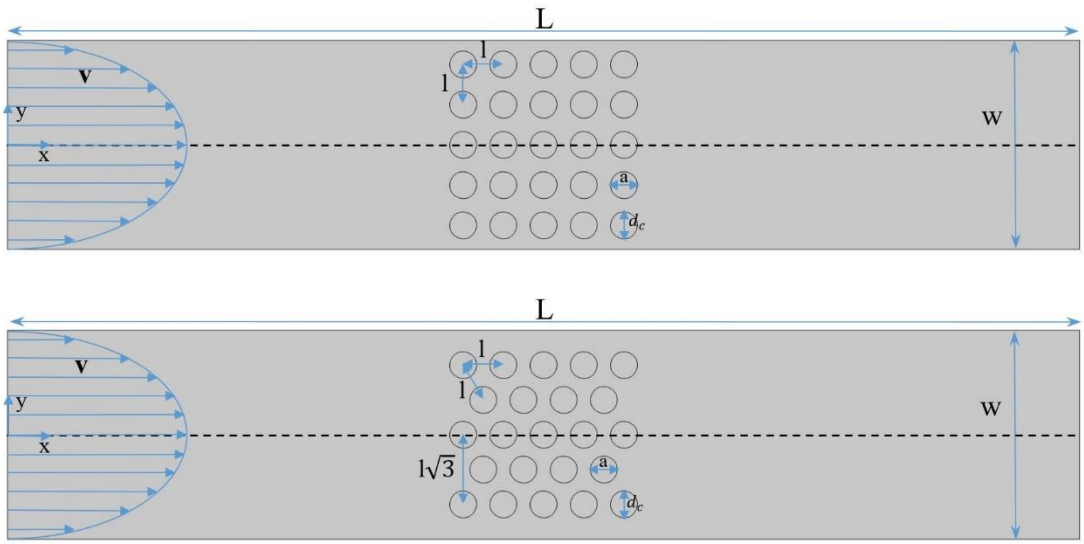

Figure 3.11 : Schematic models of the circular posts arrays in square and equilateral triangle forms.

Table 3.7 : Properties of the model of Figure 3.11.

Parameter	Description	Value
L	Length of the channel	20 (mm)
w	Width of the channel	3.897 (mm)
l	Distance between the adjacent posts	750 (μm)
a	Characteristic length of the post	500 (μm)
d_c	Diameter of the post	500 (μm)

Schematic of the models of the square cross section posts arrays in two configurations are illustrated in Figure 3.12. The model's properties are given in Table 3.8.

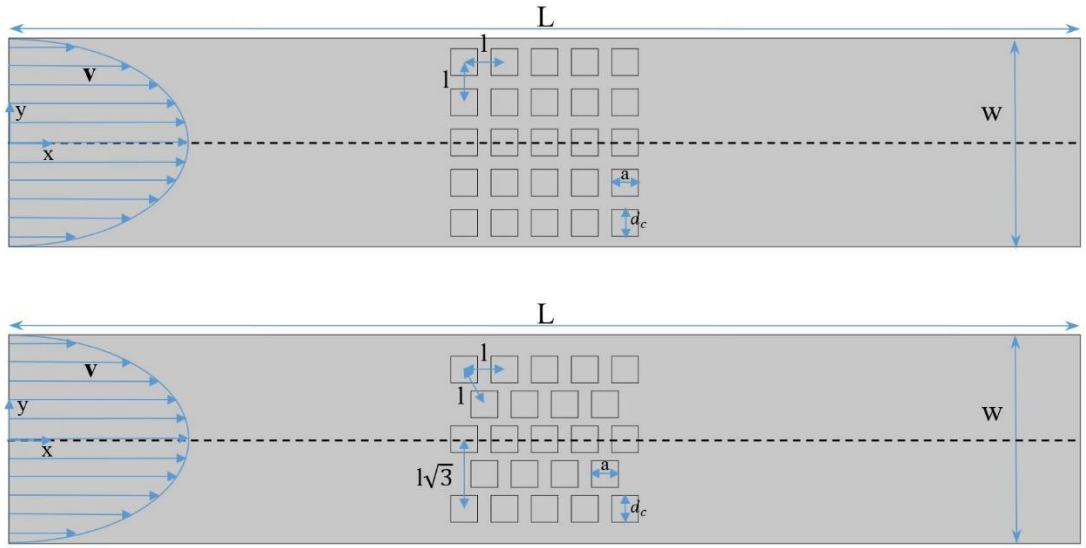

Figure 3.12 : Schematic models of the square posts arrays in square and equilateral triangle forms.

Table 3.8 : Properties of the model of Figure 3.12.

Parameter	Description	Value
L	Length of the channel	20 (mm)
w	Width of the channel	3.897 (mm)
a	Characteristic length of the post	500(μm)
l	Distance between the adjacent posts	750 (μm)
d_c	Width of the post	500 (μm)

The schematic models two configurations of the truncated hexagonal cross section posts are shown in Figure 3.13 and their properties are delivered in Table 3.9.

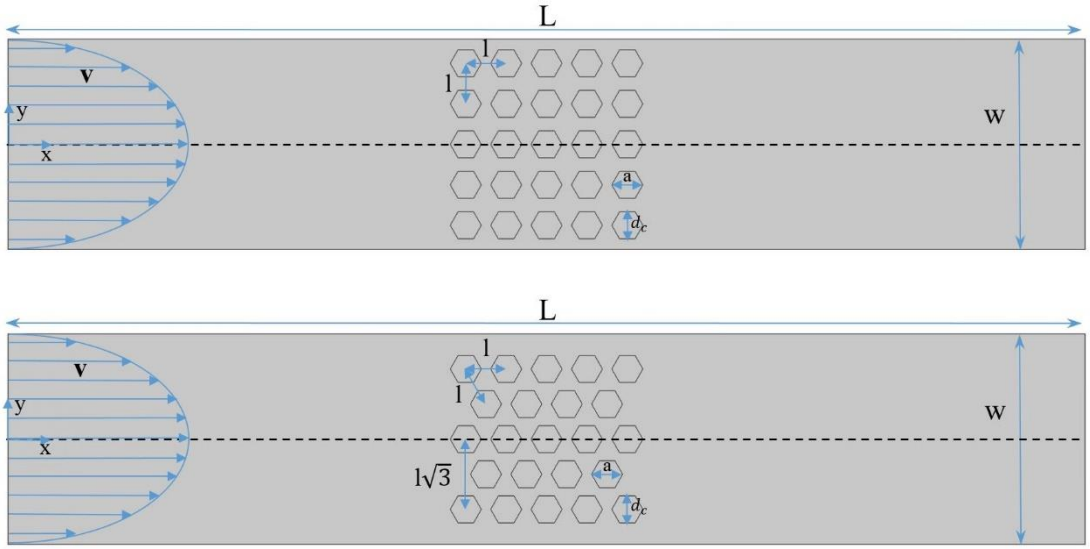

Figure 3.13 : Schematic models of the truncated hexagonal posts arrays in square and equilateral triangle forms.

Table 3.9 : Properties of the model of Figure 3.13.

Parameter	Description	Value
L	Length of the channel	20 (mm)
w	Width of the channel	3.897 (mm)
a	Characteristic length of the post	577.35 (μm)
l	Distance between the adjacent posts	750 (μm)
d_c	Width of the post	500 (μm)

Similar to the previous models, the models of different configurations of the regular hexagonal cross section posts are illustrated in Figure 3.14, and their properties are given in Table 3.10.

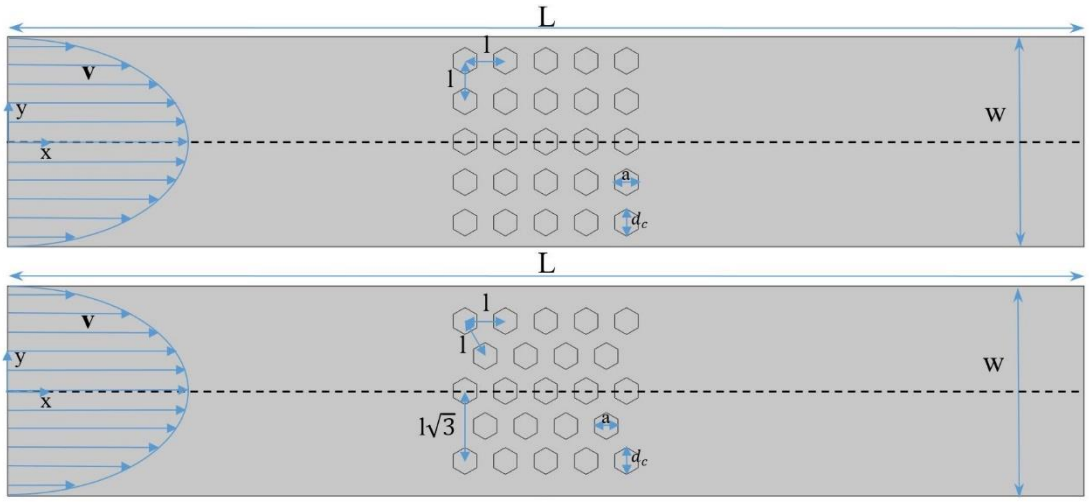

Figure 3.14 : Schematic models of the regular hexagonal posts arrays in square and equilateral triangle forms.

Table 3.10 : Properties of the model of Figure 3.14.

Parameter	Description	Value
L	Length of the channel	20 (mm)
w	Width of the channel	3.897 (mm)
a	Characteristic length of the post	433 (μm)
l	Distance between the adjacent posts	750 (μm)
d_c	Width of the post	500 (μm)

3.5 Model Definition for the Geometrical Parameters between the Posts

In addition to the configuration of the arrays, another parameter that could affect the interception efficiency is the spacing between the posts, so called the "array density." It is denoted by α/d_c where, α is the distance between centers of posts and d_c is post diameter [2].

The model is similar to the circular model of section (3.4). The reason for choosing a circular posts model is that it is more common and practical. Figure 3.15 is the schematic illustration of the model posts. Also, the necessary parameters are delivered in Table 3.11.

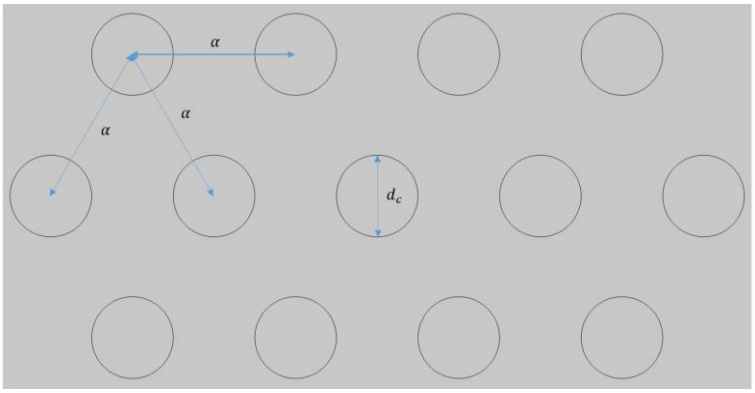

Figure 3.15 : Schematic illustration of the posts of the model.

Table 3.11 : Geometrical parameters of Figure 3.15.

Parameter	Description
α	Distance between the centers of the posts
d_c	Diameter of the post

3.6 Blood Viscosity Models

In addition to the water, in some cases, blood is used as the working fluid in order to have a more realistic vision on the field of bioparticle separation. While, in the literature, there are several models are utilized for modeling of the blood viscosity. Besides, most of the models consider the blood as a non-Newtonian fluid, in which the viscosity depends on the shear rate. In Table 3.12, properties of the blood are given [38, 39].

Table 3.12: Properties of working fluids.

Fluid	Dynamic viscosity ($Pa.s$)	Density (kg/m^3)
Blood	Variable	1050

The most common models for the viscosity of the blood are as follows:

1. Newtonian model with (equation (3.5)):

$$\mu = 0.0035\ (Pa.s) \tag{3.5}$$

2. Power law model with (equation (3.6)):

$$\mu = \mu_0 \dot{\gamma}^{n-1} \tag{3.6}$$

Where $\mu_0 = 0.035\ (Pa.s)$, $\dot{\gamma}$ is the shear rate, and $n = 0.6$.

3. Carreau model with (equation (3.7)):

$$\mu = \mu_\infty + (\mu_0 - \mu_\infty)[1 + (\lambda\dot{\gamma})^2]^{\frac{n-1}{2}} \tag{3.7}$$

Where, μ_∞ indicates the viscosity at high shear rate, which is equal to the value for the Newtonian model (i.e. $0.0035\ Pa.s$). Meanwhile, μ_0 is the viscosity at the zero shear rate that is equal to $0.056\ (Pa.s)$. In addition the values for λ and n are $3.313\ (s), 0.3568$ respectively.

4. RESULTS AND DISCUSSION

4.1 Validation of the Numerical Solutions

For validation of the accuracy of the numerical solutions, the interception efficiency of a single circular porous post inside a rectangular channel in various cases are compared with available experimental data of Chen et al. [2] Properties of the cases are given in Table 4.1.

Table 4.1 : Properties of the cases investigated by Chen et al. [2].

Case	$d_c(\mu m)$ (Post Diameter)	$d_p(\mu m)$ (Particle Diameter)	Permeability of post (m^2)	Da	Interception efficiency
1	1000	100	1×10^{-13}	1×10^{-7}	1.23
2	500	50	1×10^{-13}	4×10^{-7}	1.24
3	200	20	1×10^{-13}	2.5×10^{-6}	1.3
4	100	10	1×10^{-13}	1×10^{-5}	1.38
5	50	5	1×10^{-13}	4×10^{-5}	1.6

Simulation of the given cases is performed based on the model of the single circular porous post (i.e. extensively has been explained in section (3.2)).

Water is used as the working fluid, with the density of 1000 (kg/m^3) and the dynamic viscosity of 0.001 ($Pa.s$).

Numerical results were obtained by solving the continuity equation (4.1) and the 2-D Navier-Stokes equation (4.2) in the free media region, and the 2-D Brinkman equation (4.3) inside the porous posts, for the incompressible flow in the steady state condition. The mentioned equations are as follows:

$$(\nabla . \mathbf{v}) = 0 \tag{4.1}$$

$$\mathbf{v}.(\nabla \mathbf{v}) = -\frac{1}{\rho}\nabla P + \frac{\mu}{\rho}\nabla^2 \mathbf{v} \tag{4.2}$$

$$\nabla P = -\frac{\mu}{\kappa}\mathbf{v} + \tilde{\mu}\nabla^2 \mathbf{v} \tag{4.3}$$

Boundary conditions are identical to the model of section (3.2) (B. C. II), which are as follows:

- At the inlet (x = 0), the fully developed velocity condition $\mathbf{v} = \frac{3}{2}\mathrm{U}[1 - \left(\frac{\mathrm{y}}{\mathrm{w}/2}\right)^2]$ where, U = 0.5 (mm/s) is the average velocity, is used. This fully developed condition is mapped from the outlet of pre-calculated straight channel at the same width.
- At the walls ($y = \pm w/2$), no-slip boundary condition (i.e. $\mathbf{v} = 0$) is assumed.
- The boundary condition for the outlet ($x = L$) is zero pressure $P = 0$.
- Assumptions for the boundary conditions in the interface of the free and porous domains are the continuity in pressure $P_f = P_p$, and velocity $\mathbf{v}_f = \mathbf{v}_p$. Additionally, due to the fact that Darcy number is well below the critical value, the stress jump equals to zero.

In the work of Chen et al. [2], the values of interception efficiency were obtained for the direct interception mechanism because of its dominance in comparison with other mechanisms. In order to calculate the interception efficiency, the equation (4.4) has been used (In section 2.4 detailed explanations have been given).

$$\eta_i = \frac{b}{d_c} \tag{4.4}$$

Where, b is the span of upstream streamlines that finally pass the post with the distance less than a particle radius, and d_c is the post diameter. The span b is measured by the exported data of the numerical simulations.

Table 4.2 is the comparison of obtained values of interception efficiency of present work and the values of Chen et al. [2] and the deviation values.

Table 4.2 : Interception efficiency values of current work and by Chen et al.

Case	Interception efficiency by Chen et al. (%)	Interception efficiency by current simulation (%)	Deviation (%)
1	1.23	1.252	1.8
2	1.24	1.259	1.53
3	1.3	1.29	0.77
4	1.38	1.408	2.03
5	1.6	1.628	2.2

Figure 4.1 depicts the comparison of the interception efficiency results of Table 4.2. The deviation range is situated within the narrow range with an average deviation of 1.77 percent. Therefore, it can be concluded that the present numerical predictions are verified with reasonable accuracy.

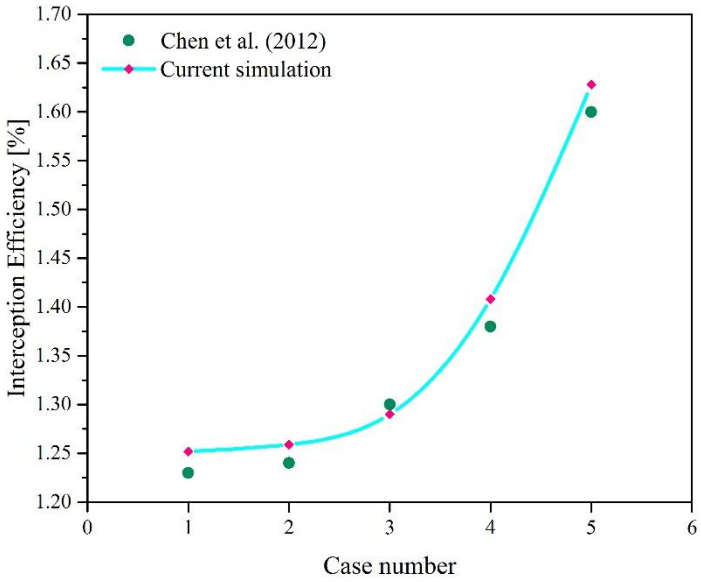

Figure 4.1 : Comparison between the interception efficiencies obtained from numerical simulations and measured by Chen et al. [2].

4.2 Comparison of the Interception efficiency of Solid and Porous Posts

In this section, numerical results of the single circular solid and porous posts models that were described in sections 3.1 and 3.2, have been compared. The values of the geometrical properties of the models are given in Table 4.3.

Table 4.3 : Geometrical properties of solid and porous posts models.

Post type	L	w	d_c
Solid	20 (mm)	2.2 (mm)	500 (μm)
Porous	20 (mm)	2.2 (mm)	500 (μm)

4.2.1 Interception efficiency of a Solid Post

In order to investigate the contribution of various factors affecting the particle interception, a real experimental condition has been assumed. For this aim, a polystyrene particle-glass post system has been considered. Meanwhile, polymeric beads such as polystyrene commonly used as particles in the experimental investigations of bioparticles. Also, to study the models based on group of

dimensionless numbers, the ratio of d_p/d_c is defined as the ratio of the diameter of the particle to the diameter of the post. Analysis is performed for the particles size of $25, 50\ (\mu m)$ corresponding to the $d_p/d_c = 0.05, 0.1$. Water is selected as the working fluid.

The governing equations and the boundary conditions for the solid post have been explained in section 3.1. The continuity equation (4.1) and the 2-D Navier-Stokes equation (4.2) for the incompressible flow in free media region numerically solved in the steady state. Additionally, boundary conditions are identical to the single circular solid model of section (3.1) (B. C. I), which are:

- At the inlet (x = 0), the fully developed velocity condition $\mathbf{v} = \frac{3}{2}\mathrm{U}[1 - \left(\frac{\mathrm{y}}{\mathrm{w}/2}\right)^2]$ where, $\mathrm{U} = 0.5\ (\mathrm{mm/s})$ is the average velocity, is used. This fully developed condition is mapped from the outlet of pre-calculated straight channel at the same width.
- At the walls $(y = \pm w/2)$ as well as the surface of the post, no-slip boundary condition (i.e. $\mathbf{v} = 0$) is assumed.
- The boundary condition for the outlet $(x = L)$ is zero pressure $P = 0$.

In the following, the explanations of determining the interception efficiency have been presented:

For calculating the direct interception efficiency, equation (4.4) has been used. As it stated previously, to obtain the thickness of upstream streamlines, numerical simulation has been performed. Accordingly, this was attained by measuring the streamlines that pass the post with a distance less than a particle radius. As a result, the values of direct interception efficiency of the solid model for $d_p/d_c = 0.05, 0.1$ are given in Table 4.4. Figure 4.2 schematically shows the thickness of the upstream streamlines.

Table 4.4 : Values of direct interception efficiency for the solid post.

Particle	25 (μm) or $(d_p/d_c = 0.05)$	50 (μm) or $(d_p/d_c = 0.1)$
Direct interception efficiency (%)	0.319	1.232

Figure 4.2 : Schematic illustration of the streamlines around the solid post with the distance less than 25(μm) inside the channel.

The contribution of Brownian diffusion for the particle sizes of $25, 50$ (μm) can be neglected. Because its effect is significant for particles smaller than $1, 2$ (μm).

In order to study the influence of Inertial impaction, the Stoke's number (equation (4.5)) has been calculated. To clarify, it shows the importance of the effect of inertial impaction:

$$Stk = \frac{1}{9} Re \left(\frac{d_p}{d_c}\right)^2 (s - 1) \tag{4.5}$$

For $Re = 10$, $d_p/d_c = 0.05$, and $s = 1.05$ for polystyrene particles [40] the value of Stoke's number is 1.38×10^{-4}, and similarly for $d_p/d_c = 0.1$ is 5.55×10^{-4}. Therefore, the influence of inertial impaction is negligible because the calculated values are less than 0.125 (based on [33]).

The gravitational sedimentation does not affect the interception efficiency since the orientation of posts is vertical.

The adhesion coefficient N_{Ad} (equation (4.6)) indicates the dominance of the near-surface effects. To explain, for small values of the adhesion coefficient, the hydrodynamic resistance effect is significant and its impact on interception efficiency must be accounted [35]. Its value can be obtained by:

$$N_{Ad} = \frac{H{d_c}^2}{9\pi\mu{d_p}^4 U A_F} \tag{4.6}$$

Where, A_F is as the following equation (4.7):

$$A_F = [2 - \ln\left(\frac{2d_c U}{\nu}\right)^{-1}] \tag{4.7}$$

The value of Hamaker constant is $0.6 \times 10^{-20} J$, which is for a polystyrene particle-glass post system [2]. The values of μ, U, and ν are 0.001 $(Pa.s)$, 0.5 (mm/s), and 10^{-6} (m^2/s) respectively.

Based on the given equations, the determined values for A_F and N_{Ad} are 0.371 and 7.32×10^{-4} for 25 (μm) particle size, and similarly for 50 (μm) particle size are 0.371 and 4.57×10^{-5}. Due to the considerable effect of hydrodynamic resistance for a solid post, the obtained value for direct interception efficiency should be modified. With this respect, the equation (4.8) is defined as adjustment or modification factor, and its value can be obtained from the Figure 2.5 [35].

$$\frac{\eta}{\eta_i} = \frac{\text{adjusted efficiency}}{\text{obtained efficiency by direct interception}} \tag{4.8}$$

The values of adjustment factor for the particle sizes of $25, 50$ (μm) based on Figure 2.5 is 0.276, 0.18 corresponding to the value of N_{Ad} equals to 7.32×10^{-4}, 4.57×10^{-5}.

Based on the given explanations about the various factors contributing to interception efficiency, the final values of interception efficiency of a single circular solid post for the particle sizes of $25, 50$ (μm) are given in Table 4.5.

Table 4.5 : Values of interception efficiency for a solid post.

Particle	25 (μm) or $(d_p/d_c = 0.05)$	50 (μm) or $(d_p/d_c = 0.1)$
Interception efficiency η (%)	0.088	0.222

4.2.2 Interception efficiency of a Porous Post

For modeling of the porous post, permeability of 1×10^{-13} and porosity of 99% has been chosen which, is for the VACNT material. While the VACNT material has the

highest positive features in terms of interception efficiency due to its higher permeability [2]. In addition, for the particles, polystyrene beads of the size $25, 50\ (\mu m)$ corresponding to the $d_p/d_c = 0.05, 0.1$, have been assumed. Similar to the previous model, the working fluid is water.

The governing equations and the boundary conditions for the single circular porous post have been described in section 3.2. The continuity equation (4.1) and the 2-D Navier-Stokes equation (4.2) for the flow in the free media region and the 2-D Brinkman equation (4.3) for the flow inside the porous posts numerically are solved in the steady state for an incompressible fluid flow. Boundary conditions are identical to the single circular porous model of section (3.2) (B. C. II), which are:

- At the inlet $(x = 0)$, the fully developed velocity condition $\mathbf{v} = \frac{3}{2}U[1 - \left(\frac{y}{w/2}\right)^2]$ where, $U = 0.5\ (mm/s)$ is the average velocity, is used. This fully developed condition is mapped from the outlet of pre-calculated straight channel at the same width.
- At the walls $(y = \pm w/2)$, no-slip boundary condition (i.e. $\mathbf{v} = 0$) is assumed.
- The boundary condition for the outlet $(x = L)$ is zero pressure $P = 0$.
- Assumptions for the boundary conditions in the interface of the free and porous domains are the continuity in pressure $P_f = P_p$, and velocity $\mathbf{v}_f = \mathbf{v}_p$. Also, the stress jump is considered as zero since Darcy number remains below critical value of 0.01.

Determining the interception efficiency of the stated model have been discussed in the following:

Similar to the solid post model, for calculation of the direct interception efficiency, equation (4.4) has been used. Meanwhile, the span of upstream streamlines is obtained from the results of numerical simulations. As a result, the values of direct interception efficiency of the porous model for $d_p/d_c = 0.05, 0.1$ are given in Table 4.6. Figure 4.3 schematically shows the thickness of the upstream streamlines.

Table 4.6 : Values of the direct interception efficiency for the porous post.

Particle	25 (μm) or $(d_p/d_c = 0.05)$	50 (μm) or $(d_p/d_c = 0.1)$
Direct interception efficiency η_i (%)	0.34	1.259

Figure 4.3 : Schematic illustration of the streamlines around the porous post with the distance less than $25(\mu\text{m})$ inside the channel.

Same as the solid post model, the effect of Brownian diffusion for the particle sizes of $25, 50\ (\mu m)$ for the porous post model is negligible, too.

In a similar manner to the solid post, to investigate the inertial impaction effect, the determined values of Stoke's number for the porous post for the particle sizes of $25, 50\ (\mu m)$ are 1.38×10^{-4}, 5.55×10^{-4} respectively. The obtained values are less than 0.125; thus, the effect of inertial impaction can be neglected for the porous post.

Similar to the solid post model, the gravitational sedimentation does not affect the interception efficiency.

In contrast to the solid post model, it is assumed that the near-surface hydrodynamic resistance for porous post model is very low, such that it can be neglected, and no adjustment is required for the direct interception efficiency [2].

According to the explanations of the affecting factors of interception efficiency, the final values of interception efficiency of the single circular porous post for the particle sizes of $25, 50\ (\mu m)$ are given in Table 4.7.

Table 4.7 : Values of the interception efficiency for the porous post.

Particle	25 (μm) or $(d_p/d_c = 0.05)$	50 (μm) or $(d_p/d_c = 0.1)$
Interception efficiency η (%)	0.34	1.259

By comparing the obtained values for the interception efficiencies of both solid and porous posts, it can be concluded that the amount of interception efficiency can

significantly be increased by using a porous post. Figure 4.4 illustrates the comparison of the interception efficiency of the solid and porous post for two ratios of the particle to post sizes of 0.05, 0.1. Additionally, the distribution for both of the ratios is similar, while with a smaller magnitude of the smaller ratio.

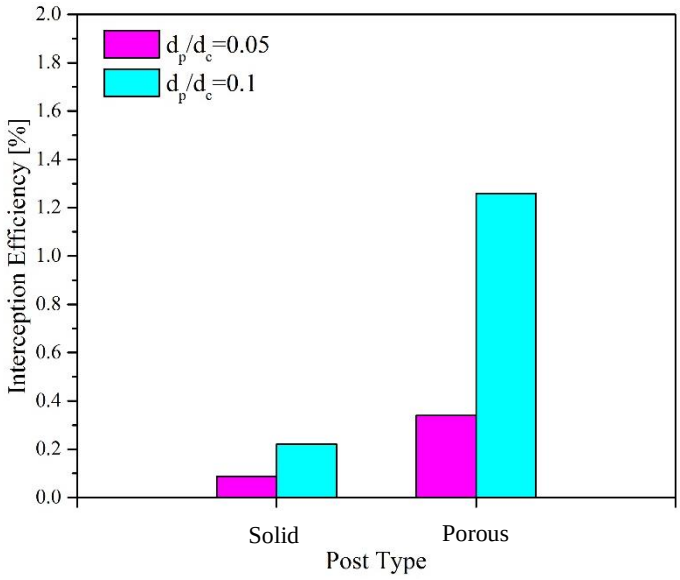

Figure 4.4 : Comparison of the interception efficiency of the solid and porous post.

4.2.3 Investigation of the Streamlines Pattern

It is expected that passing the fluid through a porous post would result in changing in flow streamlines. In this regard, Figure 4.5 shows the streamlines of a solid and a porous post. The streamlines of the porous post are depicted for $Da = 4 \times 10^{-5}$ corresponding to permeability of 10^{-11} (m^2) and characteristic length of 500 (μm).

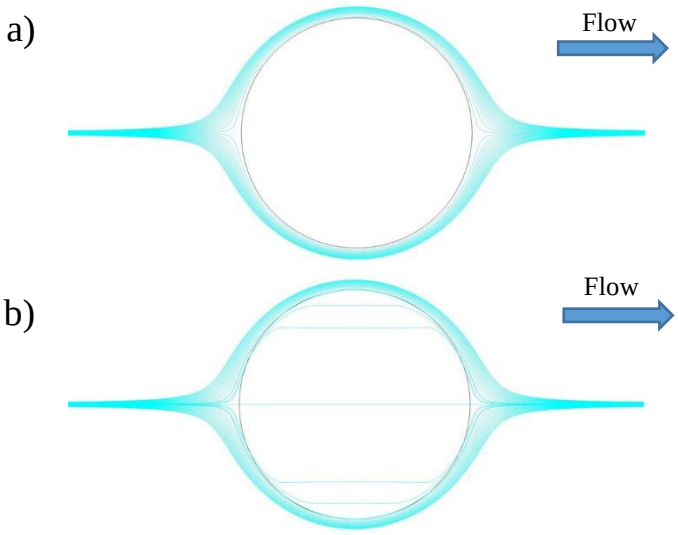

Figure 4.5 : Streamlines comparison for a) a solid post and b) a porous post.

It can be observed that streamlines around the porous post are concentrated in areas near to the post surface than the streamlines around the solid post. Furthermore, it is observable that some streamlines pass through the porous post, and they are tightened around it. Consequently, many more streamlines can pass through the porous post and the thickness of the upstream streamlines is higher. In other words, the interception efficiency of the porous post will be higher.

It is noteworthy that for the rest of the investigations of this thesis, porous material has been chosen due to its impact on the improvement of interception efficiency. Moreover, the evaluation of interception efficiency is performed for the direct interception mechanism, and other mechanisms have been neglected due to their insignificant effect on interception efficiency of a porous post.

4.3 Investigation of the Effect of the Darcy Number:

Darcy number (equation (4.8)) is a key factor in the studies of porous media.

$$Da = \frac{\kappa}{a^2} \tag{4.8}$$

The model is based on the model of a single circular porous post (section 3.2). Also, investigations are for water as the working fluid.

4.3.1 Effect of Darcy number on different post diameter

The model has been studied in the three cases a, b, and c. Figure 4.6 schematically illustrates the posts of these cases, and properties of them are delivered in Table 4.8. The governing equations and the boundary conditions are identical to the single circular porous post of section (4.2.2).

Figure 4.6 : Schematic illustration of posts of models a) $5\mu m$, b) $50\mu m$ and c) $500\mu m$.

Table 4.8 : Properties of the cases.

Case	L (Length of the channel)(mm)	w (Width of the channel)(mm)	d_c (Characteristic length)(μm)	Porosity (%)	Permeability of post (m^2)	Da (Darcy number)
a	20	2.2	5	99	10^{-13}	0.004
b	20	2.2	50	99	10^{-11}	0.004
c	20	2.2	500	99	10^{-9}	0.004

The goal of developing these cases is to investigate the effect of a constant Darcy number on streamlines pattern for different porous posts characteristics. The Darcy number indicates the accessibility of fluid inside porous structures. Thus, for a constant Darcy number in several cases, the same level of fluid accessibility should be achieved. Figure 4.7 confirms that for an equal Darcy number, the level of the accessibility is the same (i.e. the patterns of the streamlines through the posts are the same).

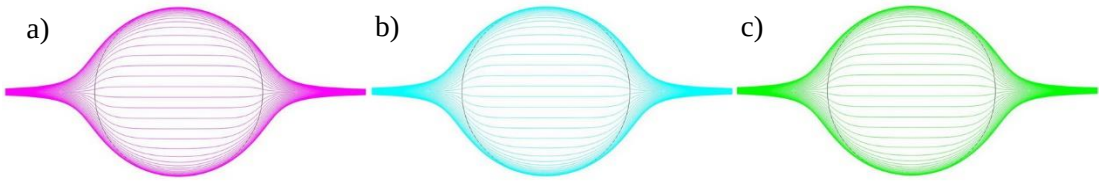

Figure 4.7 : Illustration of the constant Darcy number effect on streamlines pattern for different post sizes. (For better comparison, the smaller posts are scaled to the same size as the largest one.).

4.3.2 Effect of the Darcy number on interception efficiency

The model has been investigated in the four cases a, b, c, and d. Properties of these cases are given in Table 4.9. The governing equations and the boundary conditions are as the same as the single circular porous post of section (4.2.2).

Table 4.9 : Properties of the cases.

Case	L (Length of the channel)(mm)	w (Width of the channel)(mm)	d_c (Characteristic length)(μm)	Porosity (%)	Permeability (m^2)	Da (Darcy number)
a	20	2.2	500	99	2.5×10^{-14}	10^{-7}
b	20	2.2	500	99	2.5×10^{-12}	10^{-5}
c	20	2.2	500	99	2.5×10^{-10}	10^{-3}
d	20	2.2	500	99	2.5×10^{-8}	10^{-1}

The interception efficiency has been obtained for the direct interception, and other mechanisms of interception have been neglected. Figure 4.8 depicts the interception

efficiency with respect to different Darcy numbers, for two ratios of particle to post diameter (d_p/d_c= 0.05 and 0.1). It should be pointed out that the interception efficiency increases by the Darcy number. More important, obtained curves indicate that the increment in interception efficiency is not linear. These curves can be explained by three ranges of Darcy number:

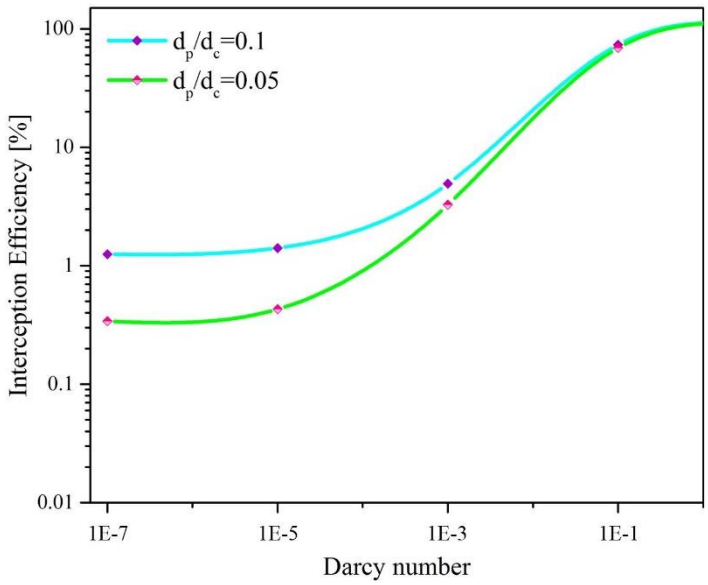

Figure 4.8 : Impact of the different Darcy number on interception efficiency.

1) For the range of $10^{-7} < Da < 10^{-4}$, by increasing Darcy number small increasing in the interception efficiency occurs.
2) For the range of $10^{-4} < Da < 10^{-2}$ much greater increment in the interception efficiency happens by increasing the Darcy number.
3) For $Da > 10^{-2}$ there is an asymptotical approach in interception efficiency to 100%.

4.4 Effect of the Different Materials of the Porous Post

One of the parameters that could affect the interception efficiency, is the material used for the posts. Previously, in the comparison between a solid and porous post, it was observed that higher interception efficiency could be achieved due to the use of the porous material. The reason for higher interception efficiency is resulting from the increased thickness of upstream streamlines of the flow, due to much more penetration of them inside the porous structure. However, different porous materials have different permeabilities. Therefore, according to Darcy number and given explanations in the

previous section (4.3.2), the more permeable material results in the higher interception efficiency. In Table 4.10, three types of porous materials with three different orders of magnitude of permeabilities are given.

Figure 4.9 illustrates the variation of interception efficiency with respect to the Darcy number of the given materials for the two particles to post ratios of 0.05 and 0.1. It can be observed that by utilizing the porous material of VACNT, higher interception efficiency is achieved.

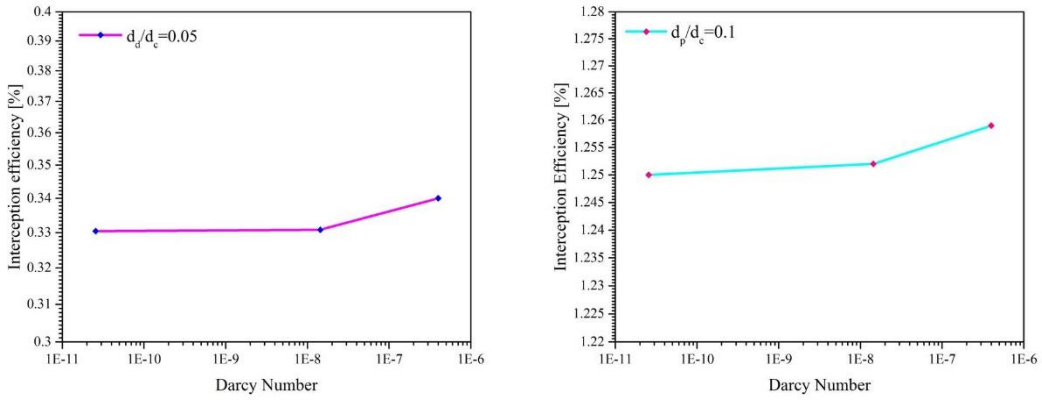

Figure 4.9 : Interception efficiency of various porous materials for $d_p / d_c = 0.05, 0.1$.

Table 4.10 : Properties of the various materials used for the porous post [13].

Material	Permeability κ (m^2)	Da (Darcy number)
Porous Silicon	6.4×10^{-18}	2.56×10^{-11}
Porous Membranes	3.6×10^{-15}	1.44×10^{-8}
VACNT	1×10^{-13}	4×10^{-7}

4.5 Influence of the Shape of the Porous Post

In this part, the effect of posts' shape variation on particle interception has been investigated. This aimed to find the optimal post shape with maximum interception efficiency within the models. The described models of section (3.3), which are the airfoil, truncated hexagon, square, and regular hexagon have been selected. Also, the model of the circular post of section (3.2) is included. It should be noticed that the width of the posts is equal in all of the models.

The governing equations are the continuity equation (4.1) and the 2-D Navier-Stokes equation (4.2) for the incompressible flow in free media region, and the 2-D Brinkman equation (4.3) for the incompressible flow inside the porous posts that are numerically

solved for the steady state. The boundary conditions are identical to the model of the single circular porous post (B. C. II).

Two factors of the various geometries affect the interception efficiency. The first one is the characteristic length of the porous post (i.e. a parameter of Darcy number). To explain, the smaller characteristic length results in the higher Darcy number, which leads to a higher interception efficiency. The second factor is the effect of drag of a post (i.e. the drag on a post as a result of the shape of the post). In other words, the drag alters the streamlines around the post; thus, it would change interception efficiency of the posts.

Figure 4.10 depicts the magnitude of interception efficiency of two different particle sizes ($25\mu m, 50\mu m \; or \; d_p/d_c = 0.05, 0.1$) for posts with five different cross sections. The water is chosen for the working fluid, and the VACNT material has been selected for the posts. It is clear that the post with regular hexagon shape has the highest figures; whereas the post with cross section of airfoil has the lowest one. As a result, it can be conclude that the regular hexagon shape has the best positive feature in terms of particle interception.

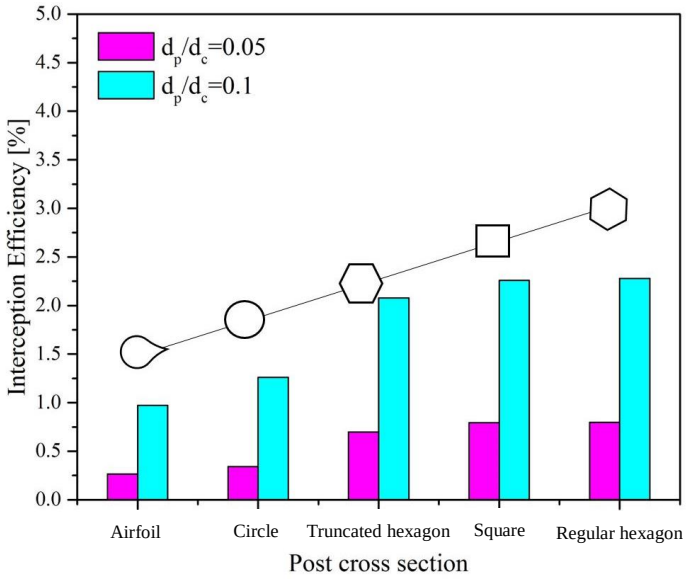

Figure 4.10 : Interception efficiency of the post with different shapes for water as working fluid.

This outcome is resulted from the combined impact of two underlying mentioned factors namely characteristic length of the post and drag resulted from the shape of the post. Meanwhile, the hexagonal shape with the lowest characteristic length would have the highest interception efficiency.

Figure 4.11 depicts the magnitude of interception efficiency of particle sizes of $25, 50\mu m \; or \; d_p/d_c = 0.05, 0.1$ for posts with five different cross sections. Results are for blood as a working fluid including non-Newtonian fluid characteristics, and the VACNT material has been chosen for the posts. Power law model utilized for modeling of blood around the posts, while the Newtonian model is applied for simulation of flow inside the porous structure. It is remarkable that utilization of blood considerably increases the interception efficiency, being approximately 60 percent.

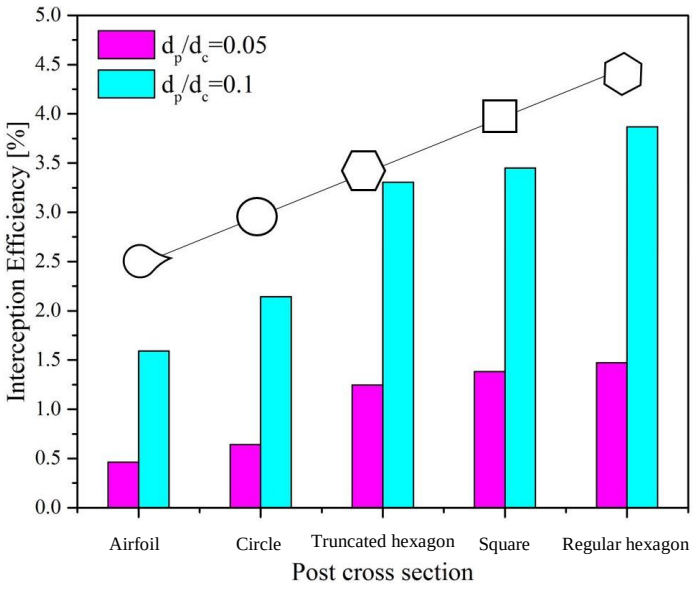

Figure 4.11 : Interception efficiency of the post with different shapes for the blood as working fluid.

Investigation of the streamlines pattern: In Figures 4.12-4.16 schematics of the streamlines patterns have been depicted for various cross sections with permeability of 10^{-11} (m^2) for water and blood. It is clear that the utilization of blood as the working fluid allows many more streamlines to penetrate inside the post, which means that higher interception can be achieved.

a) b)

Figure 4.12 : Schematic of the flow streamlines of an airfoil post for a) water b) blood.

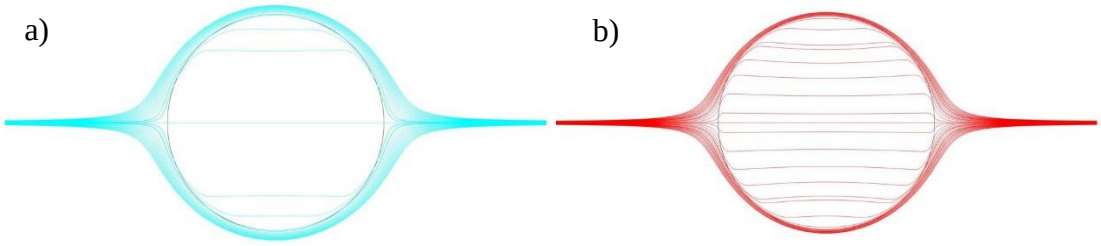

Figure 4.13 : Schematic of the flow streamlines of a circular post for a) water b) blood.

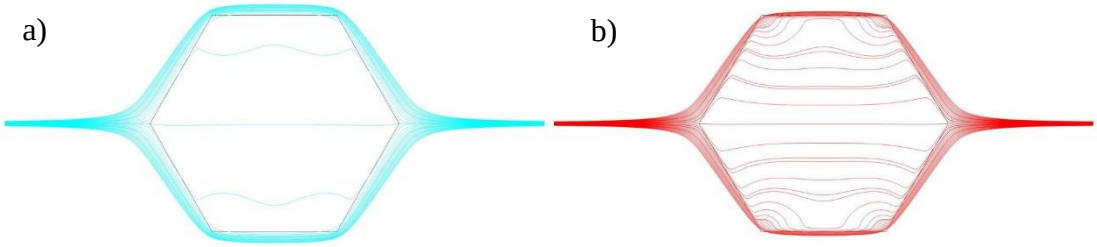

Figure 4.14 : Schematic of the flow streamlines of a truncated hexagon post for a) water b) blood.

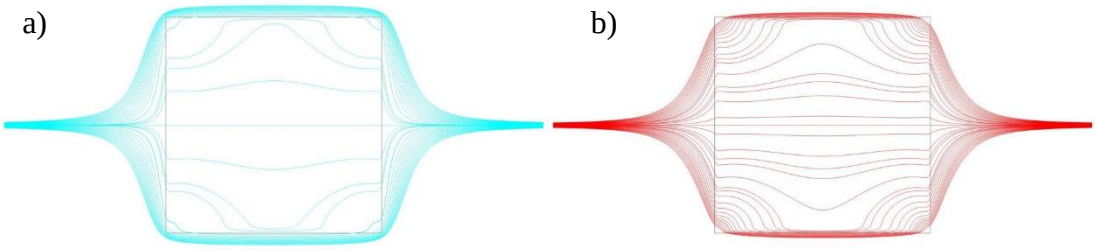

Figure 4.15 : Schematic of the flow streamlines of a square post for a) water b) blood.

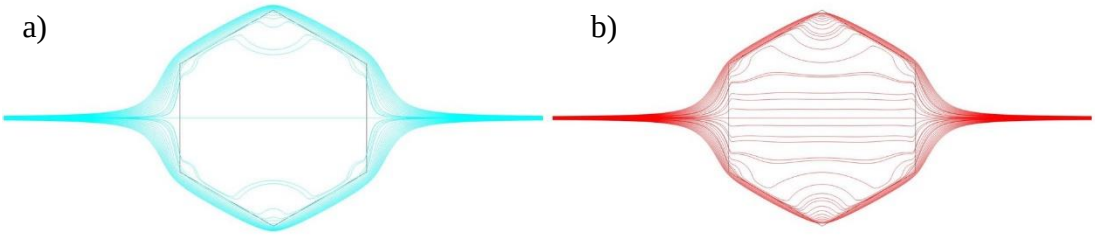

Figure 4.16 : Schematic of the flow streamlines of a regular hexagon post for a) water b) blood.

4.6 Impact of the Configuration of the Porous Posts

In order to investigate this issue, models of the section (3.4) have been chosen. It should be mentioned that the governing equations and the boundary conditions are as the section (4.5). Furthermore, the interception efficiency is determined for a post positioned in the center of the front row in the array, in each model.

Figure 4.17 and Figure 4.18 compare the magnitude of interception efficiency within two configurations with various post cross sections including circular, square, and hexagonal for water as a working fluid and the VACNT material for the posts. It can be concluded that the square configuration is the best choice regarding the interception efficiency with the highest value. Additionally, the square configuration of the hexagonal post has the highest value as compared to the other cross sections. Also, there is another impressive feature in the equilateral triangle configuration. To clarify, the circular cross section experiences improvement in interception efficiency.

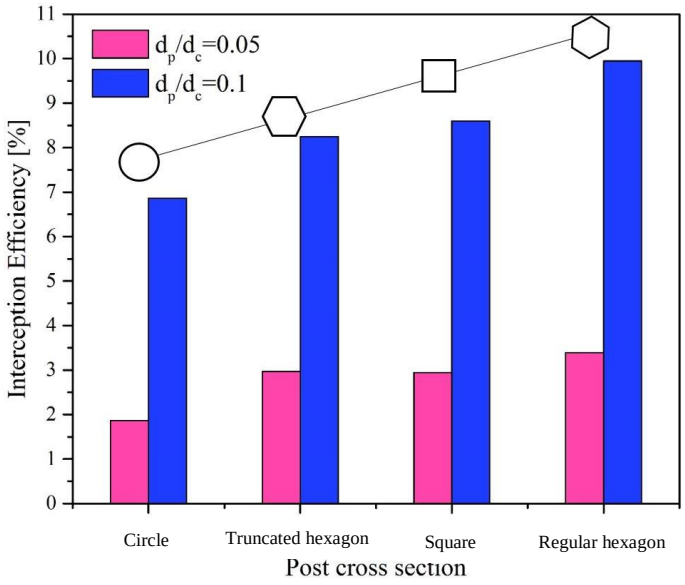

Figure 4.17 : Interception efficiency of the post arrays in the square configuration for water.

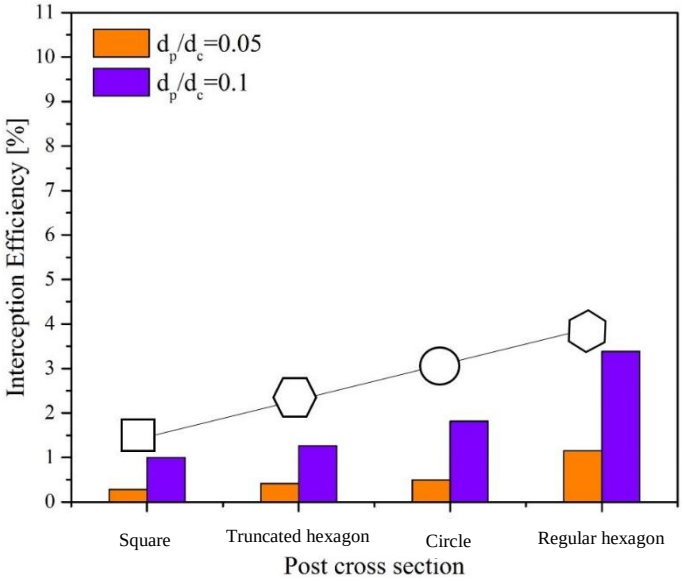

Figure 4.18 : Interception efficiency of the post arrays in the equilateral triangle configuration for water.

Figure 4.19 and Figure 4.20 are the comparisons of interception efficiencies of different cross sections for the two configurations for blood as the working fluid and the VACNT material for the posts. It is important to emphasize the fact that the interception efficiency experiences upward trend similar to the result of water; whereas, the interception efficiency of blood is higher than the results for water in all configurations.

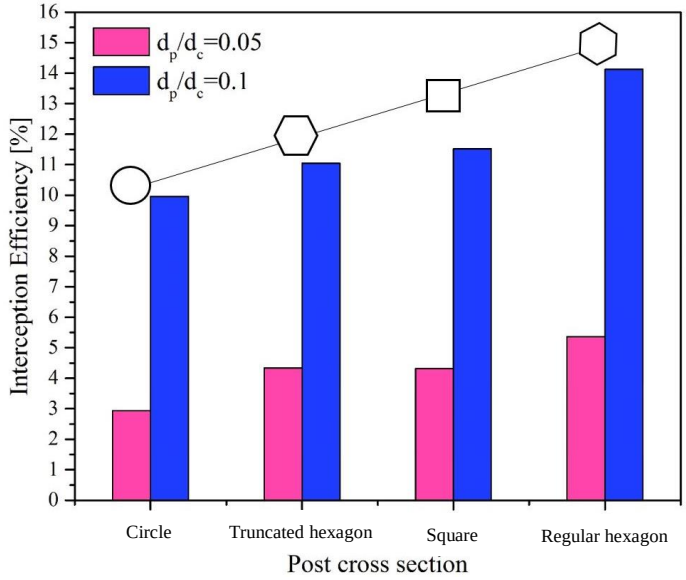

Figure 4.19 : Interception efficiency of the post arrays in the square configuration for blood.

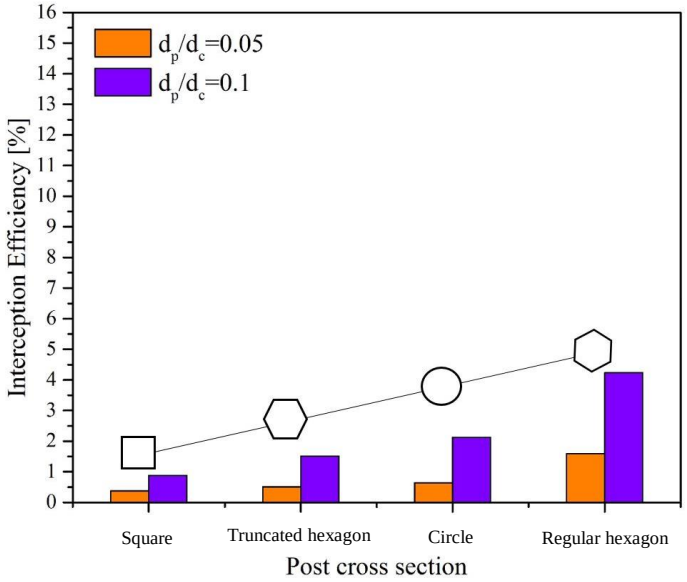

Figure 4.20 : Interception efficiency of the post arrays in the equilateral triangle configuration for blood.

Furthermore, the interception efficiencies in the square configuration have a higher magnitude in comparison with equilateral triangle configuration. Additionally,

interception efficiency of the hexagonal post has the highest value in both configurations.

Investigation of the streamlines pattern: Figures 4.21-4.22 schematically illustrate the distribution of flow streamlines within hexagonal post arrays (which has highest interception efficiency) for two configurations respectively for water and blood. The depicted streamlines are for permeability of $10^{-9}\,(m^2)$. It is clear that the concentration of streamlines within square configuration increases as compared to the equilateral triangle configuration and they are squeezed between the posts. As a result, interception efficiency is higher for square configuration. In addition, there is another interesting point that is for a high permeability like $10^{-9}\,(m^2)$ the deviation of streamlines inside the posts are very low.

a)

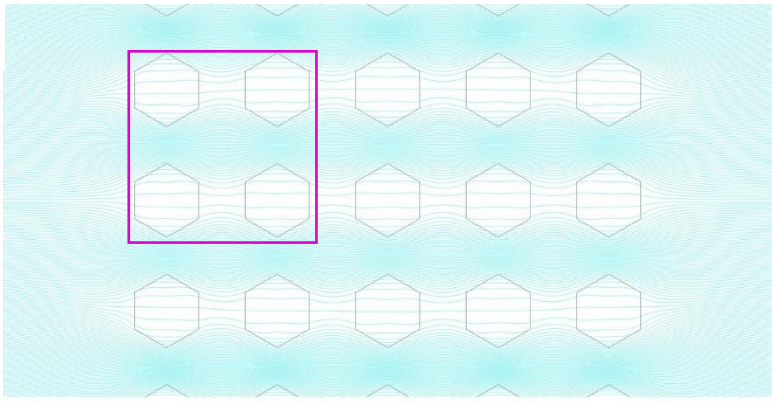

b)

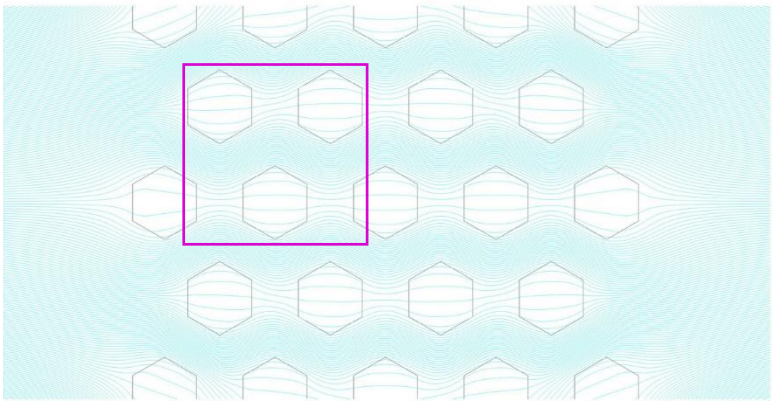

Figure 4.21 : Plots of streamlines for post arrays with the regular hexagonal cross section for water. a) Square configuration b) Equilateral triangle configuration. The boxes indicate a higher concentration of streamlines for the square configuration.

As it is expected, for blood the penetration of streamlines inside the post are more in comparison with water, and it is the reason for higher interception efficiency when blood is used.

a)

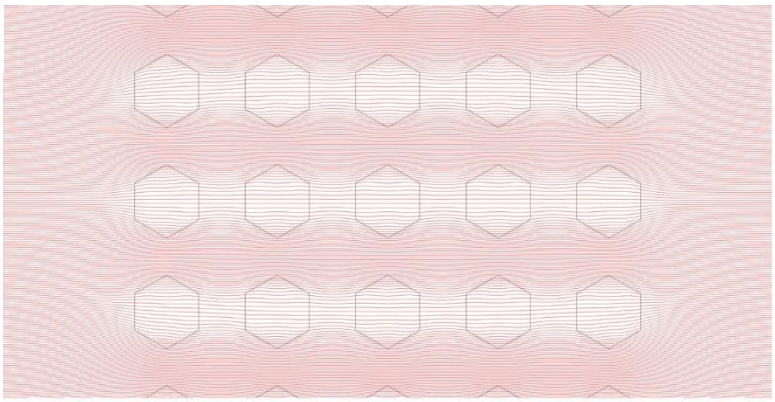

b)

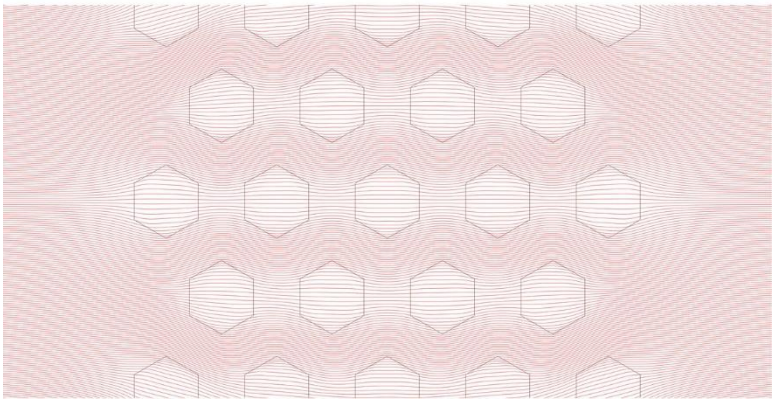

Figure 4.22 : Plots of streamlines for post arrays with the regular hexagonal cross section for blood. a) Square configuration b) Equilateral triangle configuration.

4.7 Effect of the Geometrical Parameters between Posts

In order to investigate this issue, the model of the section (3.5) has been chosen. The governing equations and the boundary conditions are as the section (4.5). Water has been chosen as the working fluid, and the material of the posts are VACNT.

The interception efficiency is determined for the post located in the center of the front row within the array. Figure 4.23 depicts the variation of interception efficiency with respect to the dimensionless parameter called array density with the values of 1.5, 2, 3, 5, and 6. It is clear that the interception efficiency experiences step decrease with the variation of array density. It stems from the fact that there is lower penetration of flow through the posts. In other words, the squeeze of streamline to the surface of the post reduces due to the reduction of neighbor posts' impact. Additionally, there is an interesting variation in the slope of interception efficiency at higher values of array density. To explain, there is not a significant change in the interception efficiency.

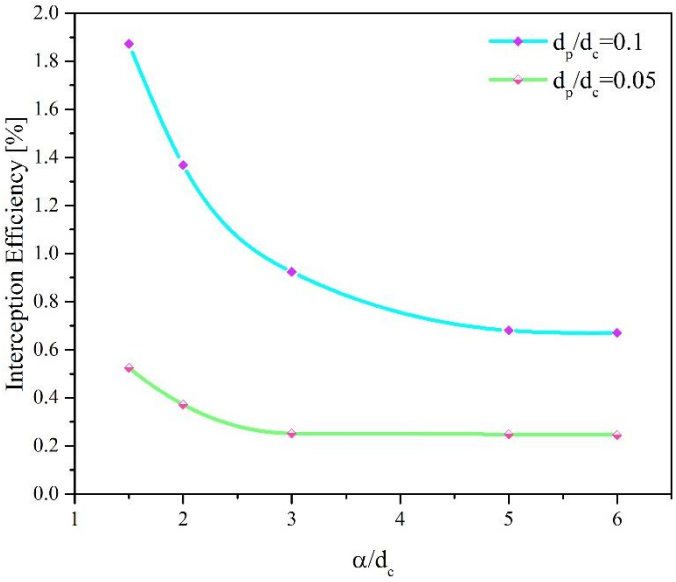

Figure 4.23 : Variation of interception efficiency versus array density.

5. CONCLUSION

Particle separation mechanism with micro-pillars (posts) method has been investigated for flow within channels with integrated posts. In this respect, the impact of underlying parameters such as the material of posts, shape of the post, different configuration of post arrays, and geometrical properties of arrays have been evaluated. Additionally, to develop the investigations to include various fluid types, water is utilized representing a Newtonian fluid, and blood employed as a non-Newtonian fluid.

Initially, the solid post is compared with the post including porous features in terms of the vital parameter of interception efficiency. Then the impact of the porous materials physical properties is examined. In addition, the posts with various cross sections ranging from airfoil type to hexagonal ones are compared. Then, the models with a combination of a set of the posts are developed that is more close to the practical applications. Finally, the influence of geometrical parameters governing micro-pillar arrays is explored.

The comparison of the solid post with porous one enlightened the point that post with porous features has a higher Interception efficiency. This issue is resulting from the negligible hydrodynamic resistance of the porous post. Moreover, investigation of post's physical properties indicated that posts with higher permeability would have higher interception efficiency. This issue stems from higher Darcy number that is the primary factor in interception efficiency. Furthermore, it is observed that the regular hexagonal post shows higher interception efficiency due to the lower characteristic length that has a direct impact on the Darcy number. Finally, it is found out that the square configuration of regular hexagonal posts has higher interception efficiency as compared to equilateral triangle configuration. This issue is resulting from the squeezes of streamlines within posts. Besides, in order to expand the investigation realm to include more practical applications, blood is studied as well. This investigation revealed that blood as a working lead to higher interception efficiency as opposed to water.

The complicated mechanism of flow through the posts requires a more detailed investigation along with the experimental evaluations, to form a solid knowledge of practical applications. Additionally, for the prospective investigator, evaluation of the shape and posts configurations for finding the optimal cases can be recommended.

6. REFERENCES

[1] **Chen, G. D., Fachin, F., Fernandez-Suarez, M., Wardle, B. L., Toner, M.** (2011). Nanoporous elements in microfluidics for multiscale manipulation of bioparticles. *Small*;7,8. p: 1061-7.

[2] **Chen, G. D., Fachin, F., Colombini, E., Wardle, B. L., Toner, M.** (2012). Nanoporous micro-element arrays for particle interception in microfluidic cell separation. *Lab Chip*;12,17. p: 3159-67.

[3] **Neale, G., Epstein, N., Nader, W.** (1973). Creeping flow relative to permeable spheres. *Chemical Engineering Science*;28,10. p: 1865-74.

[4] **Drott, J., Rosengren, L., Lindström, K., Laurell, T.** (1999). Porous silicon carrier matrices in micro enzyme reactors-influence of matrix depth. *Microchimica Acta*;131,1-2. p: 115-20.

[5] **Vanni, M.** (2000). Creeping flow over spherical permeable aggregates. *Chemical Engineering Science*;55,3. p: 685-98.

[6] **Sutherland, D., Tan, C.** (1970). Sedimentation of a porous sphere. *Chemical Engineering Science*;25,12. p: 1948-50.

[7] **Singh, M., Gupta, J.** (1971). The flow of a viscous fluid past an inhomogeneous porous cylinder. *ZAMM-Journal of Applied Mathematics and Mechanics/Zeitschrift für Angewandte Mathematik und Mechanik*;51,1. p: 17-25.

[8] **Tufenkji, N., Elimelech, M.** (2004). Correlation equation for predicting single-collector efficiency in physicochemical filtration in saturated porous media. *Environmental science & technology*;38,2. p: 529-36.

[9] **Shahsavari, S., Wardle, B. L., McKinley, G. H.** (2014). Interception efficiency in two-dimensional flow past confined porous cylinders. *Chemical Engineering Science*;116. p: 752-62.

[10] **Shi, Y.-Y., Braden, R. E.** (1966). The effect of permeability on low Reynolds number flow past a circular porous cylinder. *Dev theor appl Mech*;3. p: 761-75.

[11] **Bhattacharyya, S., Dhinakaran, S., Khalili, A.** (2006). Fluid motion around and through a porous cylinder. *Chemical Engineering Science*;61,13. p: 4451-61.

[12] **Yu, P., Zeng, Y., Lee, T. S., Chen, X. B., Low, H. T.** (2011). Steady flow around and through a permeable circular cylinder. *Computers & Fluids*;42,1. p: 1-12.

[13] **Chen, G. D.** (2012). Nanoporous elements in microfluidics for multi-scale separation of bioparticles: MASSACHUSETTS INSTITUTE OF TECHNOLOGY.

[14] **Bhagat, A. A. S., Kuntaegowdanahalli, S. S., Papautsky, I.** (2008). Enhanced particle filtration in straight microchannels using shear-modulated inertial migration. *Physics of Fluids (1994-present)*;20,10. p: 101702.

[15] **Di Carlo, D., Irimia, D., Tompkins, R. G., Toner, M.** (2007). Continuous inertial focusing, ordering, and separation of particles in microchannels. *Proceedings of the National Academy of Sciences*;104,48. p: 18892-7.

[16] **Russom, A., Gupta, A. K., Nagrath, S., Di Carlo, D., Edd, J. F., Toner, M.** (2009). Differential inertial focusing of particles in curved low-aspect-ratio microchannels. *New journal of physics*;11,7. p: 075025.

[17] **Gossett, D. R., Weaver, W. M., Mach, A. J., Hur, S. C., Tse, H. T. K., Lee, W., et al.** (2010). Label-free cell separation and sorting in microfluidic systems. *Analytical and bioanalytical chemistry*;397,8. p: 3249-67.

[18] **Davis, J. A., Inglis, D. W., Morton, K. J., Lawrence, D. A., Huang, L. R., Chou, S. Y., et al.** (2006). Deterministic hydrodynamics: taking blood apart. *Proceedings of the National Academy of Sciences*;103,40. p: 14779-84.

[19] **Voldman, J., Gray, M. L., Toner, M., Schmidt, M. A.** (2002). A microfabrication-based dynamic array cytometer. *Analytical chemistry*;74,16. p: 3984-90.

[20] **Kovac, J., Voldman, J.** (2007). Intuitive, image-based cell sorting using optofluidic cell sorting. *Analytical chemistry*;79,24. p: 9321-30.

[21] **Neild, A., Oberti, S., Radziwill, G., Dual, J.** (2007). Simultaneous positioning of cells into two-dimensional arrays using ultrasound. *Biotechnology and bioengineering*;97,5. p: 1335-9.

[22] **Nilsson, J., Evander, M., Hammarström, B., Laurell, T.** (2009). Review of cell and particle trapping in microfluidic systems. *Analytica chimica acta*;649,2. p: 141-57.

[23] **Chen, G. D., Alberts, C. J., Rodriguez, W., Toner, M.** (2009). Concentration and purification of human immunodeficiency virus type 1 virions by microfluidic separation of superparamagnetic nanoparticles. *Analytical chemistry*;82,2. p: 723-8.

[24] **Wang, M. M., Tu, E., Raymond, D. E., Yang, J. M., Zhang, H., Hagen, N., et al.** (2005). Microfluidic sorting of mammalian cells by optical force switching. *Nature biotechnology*;23,1. p: 83-7.

[25] (Retrieved December 2016). Affinity chromatography. Wikipedia. p. Affinity chromatography.

[26] **Murthy, S. K., Sin, A., Tompkins, R. G., Toner, M.** (2004). Effect of flow and surface conditions on human lymphocyte isolation using microfluidic chambers. *Langmuir*;20,26. p: 11649-55.

[27] **Cheng, X., Irimia, D., Dixon, M., Sekine, K., Demirci, U., Zamir, L., et al.** (2007). A microfluidic device for practical label-free CD4+ T cell counting of HIV-infected subjects. *Lab on a Chip*;7,2. p: 170-8.

[28] **Adams, A. A., Okagbare, P. I., Feng, J., Hupert, M. L., Patterson, D., Göttert, J., et al.** (2008). Highly efficient circulating tumor cell isolation from whole blood and label-free enumeration using polymer-based microfluidics with an integrated conductivity sensor. *Journal of the American Chemical Society*;130,27. p: 8633-41.

[29] **White, F. M.** (2011). Fluid Mechanics: McGraw Hill.

[30] **Nield, D. A., Bejan, A.** (2006). Convection in porous media: Springer Science & Business Media.

[31] **Ochoa-Tapia, J. A., Whitaker, S.** (1995). Momentum transfer at the boundary between a porous medium and a homogeneous fluid—I. Theoretical development. *International Journal of Heat and Mass Transfer*;38,14. p: 2635-46.

[32] **Partha, M., Murthy, P., Raja Sekhar, G.** (2005). Viscous flow past a porous spherical shell—effect of stress jump boundary condition. *Journal of engineering mechanics*;131,12. p: 1291-301.

[33] **Wessel, R., Righi, J.** (1988). Generalized correlations for inertial impaction of particles on a circular cylinder. *Aerosol Science and Technology*;9,1. p: 29-60.

[34] **Schrijver, J., Vreeken, C., Wesselingh, J.** (1981). Deposition of particles on a cylindrical collector. *Journal of Colloid and Interface Science*;81,1. p: 249-56.

[35] **Goren, S. L., O'Neill, M. E.** (1971). On the hydrodynamic resistance to a particle of a dilute suspension when in the neighbourhood of a large obstacle. *Chemical Engineering Science*;26,3. p: 325-38.

[36] **Spielman, L. A., Fitzpatrick, J. A.** (1973). Theory for particle collection under London and gravity forces. *Journal of Colloid and Interface Science*;42,3. p: 607-23.

[37] **Chen, G., Fachin, F., Toner, M., Wardle, B.** (2011). Microscale and nanoscale structures for manipulating particles. Google Patents.

[38] **Siebert, M. W., Fodor, P. S.** (2009). Newtonian and non-newtonian blood flow over a backward-facing step–a case study. *COMSOL Conference*. p: 1-5.

[39] **Johnston, B. M., Johnston, P. R., Corney, S., Kilpatrick, D.** (2004). Non-Newtonian blood flow in human right coronary arteries: steady state simulations. *Journal of biomechanics*;37,5. p: 709-20.

[40] **TECHNICAL DATA SHEET** Polybead® Polystyrene Microspheres. Polysciences, Inc. p. 1-4. http://www.polysciences.com/skin/frontend/default/polysciences/pdf/Microparticles%20Guide.pdf

CURRICULUM VITAE

Name Surname **:** Reza DARYANI

Place and Date of Birth **:** Maragheh-Iran, 03/09/1989

E-Mail **:** reza.dryn@gmail.com

EDUCATION **:**

- **B.Sc.** **:** 2012, Urmia University, Mechanical Engineering, Mechanical Engineering